Inhibiting the Dealkylation of Basic Arenes During n-alkane Direct Aromatization Reactions and Understanding the C_6 Ring Closure Mechanism

Jack S. Jarvis,[1] Jonathan H. Harrhy,[1] Aiguo Wang,[1] Takudzwa Bere,[2] David J. Morgan,[2] James H. Carter,[2] Alexander G. R. Howe,[3] Qian He,[3] Graham J. Hutchings[2] & Hua Song[1]*

[1]Department of Chemical and Petroleum Engineering, University of Calgary, 2500 University Dr NW, Calgary, Alberta T2N 1N4, Canada

[2]Cardiff Catalysis Institute, Department School of Chemistry, Cardiff University, Main Building, Park Place, Cardiff, UK CF10 3AT.

[3]Department of Materials Science and Engineering, National University of Singapore, 9 Engineering Drive 1, Block EA #03-09, 117575, Singapore

These authors contributed equally to this work.

*Corresponding author

Fax: +1 (403) 284-4852; Tel: +1 (403) 220-3792;

E-mail: sonh@ucalgary.ca

Abstract

Pt/KL is the widely accepted catalyst for aromatizing n-hexane by 1,6 ring closure but encounters deactivation issues when aromatizing higher carbon-number feeds; undergoing extensive dealkylation to give unwanted CH_4 and unselective products, as well as over-aromatization to form coke. Here, we report the use of a non-acidic MFI zeolite support, containing excess K^+ beyond ion exchange capacity, well dispersed Pt, and high Pt presence inside the pores, for maximising direct n-alkane aromatization selectivity. TGA, catalyst deactivation studies, and characterizations show that the smaller pore sizes and lack of large cages in the MFI support sterically inhibit coke formation inside the pores (0% compared to 4.9% over Pt/KL for n-octane aromatization), which also reduces dealkylation of ethylbenzene and o-xylene under mild conditions to give a more selective product distribution, 86% selectivity by weight towards C_6 ring closure compared to 27% for Pt/KL. Additionally, using NH_3-TPD, XPS,CO-DRIFTS, and STEM, we show the contribution of excess K^+ as an inhibitor of strong acid sites, an indirect Pt electron promoter through improving metal support interaction, and Pt dispersant. This work highlights the alternative use of well-understood zeolitic supports for the highly selective aromatization of n-heptane and n-octane by 1,6 ring closure, increasing the number of potential streams that can undergo direct aromatization, and providing a suitable alternative to Pt/KL.

Keywords: Aromatization, n-alkanes, KL Zeolite, MFI Zeolite, Platinum, Dealkylation

Introduction

Aromatization of alkanes is of interest because of its application in the synthesis of alternative valuable chemical feedstocks.[1] This application is becoming more important as the world accelerates towards a gasoline fuel-free future, with research focuses shifting towards alternative energy.[2] Nonetheless, effective use of alkane rich streams such as naphtha reformates[3] and Fischer-Tropsch process products[4] provides a unique opportunity to reduce fuel related pollution.

Noble metal-based catalysts, nominally metallic Pt, have been thoroughly investigated for the aromatization of alkanes because of their high activity and unique selectivity.[5-8] Since the 1980s, Pt/KL has stood out as the most selective and active catalyst for n-hexane aromatization to benzene[9] because of its non-acidic[10] and geometric characteristics[11,12] as well as its resistance to coke and sintering.[13,14] It is well known that 1,5 and 1,6 ring closure mechanisms often compete during these reactions over porous heterogeneous catalysts ,[15,16] with 1,6 ring closure being the dominant mechanism over Pt/KL.[17] The reason for this has been well hypothesised; it has been proposed that the hexane molecule is oriented in the channels of the catalyst in such a way that promotes 1,6 ring closure,[15] and that the Pt nanoparticle size contributes to the activity.[18] More recently, however, Pt localization has been shown to be a major factor contributing to the selectivity of this catalyst.[19] Although there are conflicting hypotheses for the selectivity of Pt/KL with n-hexane reactions, it is widely acknowledged that the acidity reduction is pivotal to promoting 1,6 ring closure as opposed to 1,5 ring closure and undesirable side reactions such as cracking and oligomerization.

Miller et al. showed that excess alkali addition by impregnation, beyond the limit permitted by ion exchange (IE), increased 1,6 ring closure selectivity slightly (a 1,6 to 1,5 ring closure ratio increase from 1.0 to 1.3 for Pt/KL).[12] Other works also suggest the contribution of K^+ to be more involved than just acidity reduction, by increasing the electron density of Pt species.[20]

Despite being a suitable catalyst for the conversion of n-hexane to benzene, Pt/KL encounters issues when converting higher mid-range n-alkanes such as n-heptane[21] and n-octane.[22] Jongpatiwut et al. showed that for n-octane, the dominant products are benzene, toluene, and methane[23] as opposed to ethylbenzene and o-xylene (the expected products from direct 1,6 and 2,7 ring closure respectively). This undesirable aromatic formation is postulated to be a result of ethylbenzene and o-xylene formation inside the channels, followed by dealkylation before escaping the inner pores and that this issue is coupled with quick deactivation of the catalyst by coking because the C_8 aromatics diffuse at a slower rate from the pores (compared to benzene). Dealkylation can be suppressed by the addition of secondary mesopores by desilication in alkali media to great effect but the problem persists.[14]

To design a catalyst capable of high 1,6 ring closure selectivities for n-hexane and high 1,6 and 2,7 ring closure (herein combined and denoted as C_6 ring closure) would give higher selectivities for n-heptane and n-octane without fast deactivation and in turn, broaden the ability of downstream refineries to produce valuable chemical precursors. It would also permit the use of a single catalyst for a wider process stream, reducing costs and enabling the industry to move away from gasoline improvement and towards chemical precursor production. The application of this mechanism is also more desirable for the aromatization of n-heptane and n-octane compared to n-hexane as benzene is a human carcinogen, thus, toluene and xylenes are preferred.[24] Herein, we demonstrate that a Pt/KMFI catalyst is capable of inhibiting dealkylation and coking mechanisms while increasing C_6 ring closure selectivity for C_7 and C_8 n-alkane aromatization reactions compared to Pt/KL. This effect is pronounced further still by the placement of excess potassium on the catalyst during synthesis. The resulting catalyst is then subjected to extensive intermediate studies to elucidate a detailed reaction mechanism for the aromatization of n-alkanes.

Support modification to inhibit dealkylation, a comparison of Pt/KL and Pt/KMFI

The biggest issue affecting the performance of Pt/KL catalysts is accelerated deactivation when reforming higher carbon number hydrocarbons (>C_6). This occurs through dealkylation of desired products and subsequent formation of coke precursors/components. Dealkylation is believed to occur for these higher-end hydrocarbons because of the unidimensional pores of L zeolite, resulting in poor diffusivity as products escape the pores[25] and allowing the formation of polycyclic hydrocarbons which are known precursors to coke. As mentioned earlier, desilication and dealumination of zeolites to increase mesoporosity is marginally effective at increasing diffusivity in such supports but this is not always the case and a more elegant solution is needed. MFI zeolite is also subject to coking, but the majority occurs on the external surface because the pores are too small (0.53 nm) for polycyclic hydrocarbons to form and, in turn, act as coke precursors. It also has 3D interconnecting channels, allowing alternative routes for reactants and products to enter and escape the pores respectively. This leads to much improved diffusion through the pores, unlike the restricting unidimensional pores of L zeolite.

To test this theory: n-hexane, n-heptane, and n-octane were subjected to aromatization reactions over Pt/KL and Pt/KMFI (K^+ loaded by IE) catalysts and selectivity towards C_6 ring closure was compared (**Fig. 1**). Detailed product distributions of these reactions are shown in **Table S4**. Pt was loaded as 1 wt% nominal by incipient wetness impregnation (IWI) and this loading was used throughout this work and confirmed by ICP-OES (**Table S1.**). N_2 physisorption analysis of the catalysts confirmed the typical pore volume and surface area values for both L and MFI zeolites discussed earlier (**Figure S1 and Table S2**). Potassium coordination comparisons between KL and KMFI supports were made using X-ray Absorption Spectroscopy at the potassium K-edge (**Figure S2**) to confirm K positioning in L zeolite cages after synthesis and sole K positioning at the IE sites of the MFI support. X-ray diffraction patterns (XRD) also confirmed the correct structure of synthesized MFI supports (**Figure S3**). n-hexane aromatization reactions yielded

similar C_6 ring closure selectivities for Pt/KL and Pt/KMFI catalysts (49% and 50% respectively). This is because the stability and smaller size of benzene would not result in dealkylation and so the effect of support for inhibiting this undesirable reaction is not seen. However, Pt/KMFI showed significantly improved C_6 ring closure selectivity when n-heptane and n-octane were charged (61% and 71% respectively compared to corresponding Pt/KL selectivities of 36% and 27%). A significant reduction in dealkylation, 73% and 60% reduction for n-heptane and n-octane reactions respectively, is successfully observed when compared to Pt/KL. All reactions were conducted at conversions between 21% and 28% to confirm the contribution of catalysts and basic depictions of the reactions, using n-octane as an example, are given (**Figure S4**). The reaction data for Pt/KL and Pt/KMFI when aromatizing C_6-C_8 n-alkanes is also shown as TOF (**Fig. 1b**) to exemplify the amount the of catalyst loaded for each reaction, where TOF is defined as the moles of n-alkane consumed per mole of Pt per hour. These data show that for n-hexane, n-heptane, and n-octane, Pt/KMFI exhibits higher TOF's than Pt/KL in all cases, 1300, 1160, and 908 respectively.

Catalysts were subject to Thermogravimetric Analysis-Differential Scanning Calorimetry (TGA-DSC) post reaction with n-alkanes to identify the nature of deposited species resulting from reaction (**Figure S5**). Pt/KMFI with n-octane shows a 1.2% mass loss at 337°C which is indicative of amorphous carbon and easily removable coke on the external surface of the catalyst.[26] This peak is witnessed for all n-alkane reactions over Pt/KMFI. Inactive coke species are witnessed in abundance (4.9% mass loss) on Pt/KL catalyst over n-octane at temperatures >500°C, typical of internal pore coking formed via polycyclic hydrocarbon precursors. This supports previously discussed experimental data where higher levels of dealkylation are observed over Pt/KL catalyst for n-octane reactions compared to Pt/KMFI. The same trend is seen for n-heptane although coking is reduced on both catalysts. Interestingly, the reduction in carbon deposition from n-octane to n-heptane over Pt/KL is 63%, similar to the 66% reduction in dealkylation products seen when making the same comparisons. Finally, the reaction over n-hexane shows us negligible

mass loss over the Pt/KL catalyst where no dealkylation products were observed. Combining these observations, it is reasonable to suggest that the level of dealkylation is directly related to the level of coking in Pt/KL catalysts, i.e. higher levels of dealkylation result in higher carbon deposition inside the pores. This suggestion is in agreement with the recognised dealkylation pathway of xylenes and toluene, reported to involve alkyl carbenium ion species capable of initiating coke formation by oligomerization, C_6 ring closure, and aromatization of alicyclics.[27] The peaks at 250°C, present on both catalysts, are due to a combination of remaining products adsorbed on active sites of the catalyst and the desorption of strongly adsorbed H_2O in the intricate pores which are easily adsorbed when exposed to the atmosphere.[28] The larger H_2O removal peak for Pt/KMFI could be a result of greater affinity to the MFI zeolite compared to L zeolite.

As well as being unidimensional, the channel structure of zeolite L (0.71 nm) contain cages (1.13 nm) which provide ample room for larger molecules to form, unhindered by steric constraints. We propose that these cages are large enough to allow polycyclic hydrocarbon formation which cannot escape the narrower channels because of the restrictive nature of the channel and single-file diffusion.[29] As carbon deposition occurs (resulting from dealkylation of product species), it builds up and partially blocks the pores, continuing to do so as the reaction proceeds. In contrast, MFI has smaller pore diameters than L zeolite. It is widely known that MFI catalysts show predominant carbon deposition on the external surface[30,31]and have greater diffusion efficiency because of 3D channels. These two attributes are demonstrated here; with reduced coking due to narrower pore diameters, which do not allow large polycyclic species to form in the pores, and reduced dealkylation of toluene and ethylbenzene/o-xylene for n-heptane and n-octane reactions respectively. We suggest that small levels of dealkylation still occurs over the Pt/KMFI catalyst due to the smaller pore sizes, however, the absence of both strong Brønsted acid sites and high H_2 partial pressures prevents secondary dealkylation reactions and thus may suppress coke

formation inside the pores.[32] The aromatization of n-alkanes (C_6-C_8) with Pt/KMFI is shown to be significantly more effective than that over Pt/KL and dealkylation is shown to be directly related to coke formation inside the pores of Pt/KL catalysts. This is likely a result of active alkyl radical formation during dealkylation; species that are prone to polymerize and subsequently form coke.[33]

Effect of Pt localization and reduction

For the previous reactions and hereafter, Pt was loaded to the supports by IWI using a modified procedure from Graaf et al. reported to promote Pt localization within the micropores of MFI[34] (**Figures S6c and S6d**). To demonstrate the importance of both Pt location and oxidation state, an alternative Ion exchange synthesis method was used with the absence of a reduction step.[35] This resulted in poor dispersion and heavy Pt loading on the external surface of the support (**Figures S6a and S6b**). It should be noted that the only change in the synthesis was through the Pt loading technique, support synthesis to achieve KMFI was identical for both catalysts. The resulting Pt/KMFI (Pt-IE) catalyst was subsequently subjected to the same reaction as those shown in **Fig. 1** and compared to its Pt/KMFI (Pt-IWI) counterpart (**Fig. 2a.**) engaged in the aforementioned reactions. Detailed product distribution for the Pt/KMFI (Pt-IE) reaction is shown in **Table S5**. The nature of the Pt particles was found to have a significant effect on the performance when aromatizing n-octane. The Pt/KMFI (Pt-IE) reaction witnesses pre-isomerisation and cracking which is not seen over Pt/KMFI (Pt-IWI). It should be noted that the Pt/KMFI (Pt-IE) catalyst was far less active than Pt/KMFI (IWI), requiring greater than a two-fold increase in catalyst weight loading to achieve a similar conversion (19% and 25% respectively). This poor catalytic performance may be a result of the significantly increased particle sizes and poorer dispersion in comparison to the Pt/KMFI (Pt-IWI) catalyst. Furthermore, the observed reduction in aromatic selectivity over Pt/KMFI (Pt-IE) could also be a result of heavy Pt clustering on the external surface as opposed to finely dispersed Pt nanoparticles which can potentially localize inside the pores. Analysing the Al 2p and Pt 4f regions of the catalysts using X-ray

photoelectron spectroscopy (XPS) allows the identification of species' electronic states in detail (**Fig. 2b.**). Pt/KMFI (Pt-IWI) shows a large peak at 74.17 eV which, upon deconvolution, reveals the Al 2p and Pt^0 $4f_{5/2}$ contributions and a third peak (Pt^0 $4f_{7/2}$) is noted at 70.62 eV.[36,37] This confirms the presence of metallic Pt species on this catalyst. Additionally, no peaks attributable to oxidized Pt species were observed for Pt indicating that metallic Pt is the predominant species, in agreement with STEM observations. Notably, the XPS spectrum of Pt/KMFI (Pt-IE) contains multiple peaks attributed to both metallic and higher energy, oxidized Pt species. Indeed, there are distinct peaks at 77.51 eV, 75.37 eV, and 71.99 eV which are attributed to Pt* $4f_{5/2}$, Pt^{2+} $4f_{5/2}$, and Pt^{2+} $4f_{7/2}$ subshells respectively.[38] The Pt* species are likely Pt^{4+}.

Investigating the effect of Pt localization and chemical state of these two catalysts has revealed that the favored Pt/KMFI (Pt-IWI) catalyst preferentially loads Pt nanoparticles <2 nm in size with high concentrations of Pt single atoms and clusters, and high dispersion. The importance of these characteristics cannot be underestimated as well dispersed metallic Pt nanoparticles are the active species for catalyzing our target reactions[6] and aromatization is enhanced inside the pores, allowing steric hinderance to promote cyclization. Such small Pt nanoparticles increases the possibility for localizing inside the pores as opposed to the formation of large clusters which are far larger than the pore diameters themselves.

Potassium influence on acidity of MFI support

Having investigated the effect of Pt dispersion on the aromatization of n-alkanes, we move to demonstrate the three-fold effect (acidity reducer, dispersant, and electron-enriching of Pt species) that K has in promoting these reactions starting with its effect on acidity. When MFI supports are subject to ion exchange with K salt precursors (usually KCl or KNO_3), it is often at low dilutions to avoid adversely affecting the support. Despite the user often employing multiple exchanges, it is unlikely that all the hydrogen occupied acid sites are replaced by K, leaving the catalyst slightly acidic and aromatization reactions likely to see by-products resulting from

cracking, oligomerization, and C_5 ring closure.[39-41] In order to make further improvement, we optimise the catalyst by loading K in excess of the IE limit by the application during synthesis (K was added to precursor mixture prior to hydrothrermal synthesis of MFI support to achieve desired $mg_K/g_{catalyst}$). KCl was the neutral salt used to avoid desilication of the support during synthesis.[42] Nominal loadings of 10, 20, 30, 40, 50, and 60 $mg_K/g_{catalyst}$ were used and actual loadings shown by inductively coupled plasma-optical emission spectrometry (ICP-OES) (**Table S1**). Pt was then applied by IWI to achieve a 1 wt% loading, as in all cases during this work, and the catalysts named as Pt/KMFI (KX-10), (KX-20), (KX-30) etc. Reactions equivalent to the previous examples with n-octane were then conducted on all 6 of the KX catalysts and compared to the previously used Pt/KMFI (where K was loaded by IE) and Pt/MFI (H-type MFI with no K addition) (**Fig. 3**). Although Pt/KMFI showed reduced dealkylation compared to Pt/KL, the undesirable effect is further reduced when K is loaded in excess. However, the K amount must be above 20 $mg_K/g_{catalyst}$ to have a major effect on the product distribution and to avoid cracking and oligomerization as shown by the formation of other aromatics and alkenes over the catalyst (**Fig. 3a**). Pt/KMFI (KX-10) shows activity more indicative of bifunctional Pt/MFI over n-octane where excessive cracking and undesirable side reactions occur. As 10 $mg_K/g_{catalyst}$ is far below the point of saturation for IE (theoretical saturation = 38.8 $mg_K/g_{catalyst}$ for a SiO_2:Al_2O_3 MFI support of approximately 30), we can safely assume that the catalyst has not achieved full IE and the presence of Brønsted acid sites are still influencing the reaction. The ideal nominal K loading from these reactions over n-octane is shown to be the 40 $mg_K/g_{catalyst}$ as C_6 ring closure gradually increases up to this point (peaking at 86 wt% selectivity) and shows reduction beyond it. Dealkylation selectivity shows the reverse trend. The performance of these catalysts, taking into account the catalyst loading, is shown in **Fig. 3c**. The productivity of the Pt/KMFI (KX-40) catalyst is the highest (38.9 moles of C_6 ring closure product/kg catalyst/h), likely owing to it's superior selectivity. See **Figure S7** for information on the nominal, actual, and theoretical maximum loading of K to these series of catalysts and **Tables S6 and S7** for detailed product distributions.

NH_3-TPD profiles were obtained (**Fig. 4**) to show the contribution of acid sites over Pt/MFI, Pt/KMFI, and Pt/KMFI (KX-40) catalysts. Pt/MFI demonstrates the strongest acidity with an 80% 'difficult desorption' contribution at 396°C attributed to Brønsted acidity. With the addition of K by IE (Pt/KMFI) these sites are significantly reduced, and the desorption temperature lowered by 74°C (from 396°C to 322°C). The weaker acid sites shown by facile desorption of NH_3 species at 226°C are enhanced. Acidity of the Pt/KMFI (KX-40) catalyst is almost completely reduced and all acid sites are attributed to facile desorption (241°C). This supports the experimental observations where K on the IE catalyst has saturated most of the strong acid sites responsible for cracking, oligomerization, and C_5 ring closure but is still not able to achieve full saturation as is the case for the Pt/KMFI (KX-40) catalyst.

The deactivation of Pt/KMFI (KX-40) was assessed and compared to that of Pt/KL by reaction of n-octane under nitrogen at 400°C for 30 mins. As these reactions were conducted in batch-mode. Catalysts were washed with acetone after reaction and dried in static air at 80°C overnight before being re-used for the same reaction. This was conducted for 4 sequential recycles with the results shown in **Fig. 3d**. Pt/KMFI (KX-40) shows initial high productivity (mol C_6 ring closure product/kg catalyst/h) as noted earlier but quickly drops to 25.97 productivity followed by stable performance thereafter. This initial drop in performance is attributed to minor loss of K^+ species after the first recycle (**Table S1**). Pt/KL shows a different trend where intial productivity is 7.63, followed by a steady decline for all subsequent recycle runs where it stops at 1.22. This steady deactivation is likely due to heavy coke formation inside the pores which continues to build after each reaction. The C_6 ring closure yield as a function of WHSV for (5, 10, and 20 g g^{-1} h^{-1}) Pt/KL and Pt/KMFI (KX-40) catalysts are also provided when reacted with n-octane. Results demonstrate lower C_6 ring closure yields of 8.99, 7.43, and 5.21 wt% for Pt/KL and 20.74, 20.64, and 17.75 wt% for Pt/KMFI (KX-40) at respective WHSV's (**Figure S8).**

Potassium as a promoter to Pt nanoparticles

Strong metal support interactions (SMSI's) are commonly attributed to reducible supports such as TiO_2 and metal particles like Pt that are larger than 2 nm in diameter.[43,44] However, recent studies acknowledge the role that SiO_2 and Al_2O_3 can play when affecting the electronic properties of metals such as Pt by doping with reducible oxides.[45] Despite this, metal support interactions can still be witnessed over non-reducible supports without the addition of reducible oxides such as those used here.[46] Here we show that the addition of K to the support, MFI, can further improve the electronic properties of the active Pt species. XPS studies (**Fig. 5a**) show that upon addition of potassium, there is a significant negative shift in binding energies from 74.48 eV to 73.77 eV and from 71.13 eV to 70.42 eV for Pt^0 $4f_{5/2}$ and Pt^0 $4f_{7/2}$ subshells respectively, indicating the formation of $Pt^{\delta-}$ species upon addition of K to the support. The shift to lower binding energies marginally increases upon further addition of K when comparing Pt/MFI, Pt/KMFI, and Pt/KMFI (KX-40); suggesting an interaction between K and support to subsequently enrich the active Pt species with electrons. The complete raw, simulated, and Al 2p contributions for these samples and C 1s calibration peaks are shown in **Figure S9**. H_2-TPR analysis of Pt/MFI and Pt/KMFI (KX-40) also showed a possible interaction between Pt and the support as a result of K presence (**Figure S10**).

As a sensitive probe to identify the nature, size, location and the exposed sites of the metal particles in the zeolite, IR spectra of CO chemisorption has been extensively used.[47,48] **Fig. 5b** shows the ones collected over Pt/KMFI and Pt/KL catalysts. For Pt/KL, absorption bands were observed in two regions: 2000-2150 cm^{-1} and *ca.* 1780 - 1880 cm^{-1}. These are due to linearly-coordinated and bridged CO species, respectively.[49-51] In the case of Pt/KMFI, the linear region is made up of several species at *ca.* 2105, 2080, 2060 and 2030 cm^{-1}.[47] It has previously been reported that the species at ~2080 cm^{-1} is due to CO adsorbed on Pt^0 nanoparticles, while species at 2105 cm^{-1} have been assigned to small clusters of cationic Pt atoms.[52] **Figure S11** shows the spectra of Pt/MFI and Pt/KMFI catalysts. Pt/MFI features bands associated with Pt nanoparticles

while Pt/KMFI exhibits a shoulder at ca. 2120 cm^{-1} which is likely to due to small clusters of Pt cations,[52] further indicating that the addition of K is capable of increasing the dispersion of Pt on MFI supported catalysts and that this effect is not exclusive to LTL type zeolites.

Typical spectra of CO adsorbed on Pt/KL is characterized by bands in the region 2150 – 1900 cm^{-1} and have been widely reported.[51-55] It was reported by Han *et al.* that the frequency of the bands depends on the location of Pt on the zeolite: Bands below 2050 cm^{-1} were assigned to Pt clusters located inside the channels of the L zeolite, and the band between 2050 and 2075 cm^{-1} related to larger Pt clusters located at the pore mouth of the L zeolite. Additionally, bands above 2075 cm^{-1} represent Pt clusters located outside the L zeolite pores.[56]

Fig 5c. shows the infrared spectrum of adsorbed CO on a set of potassium-exchanged catalysts with K concentrations ranging from 10 – 60 mg/g. At the lowest potassium concentration, the infrared band for CO adsorbed on platinum consists of a main peak centred at 2073 cm^{-1} and shoulders at 2105, 2020, 2000 and 1970 cm^{-1}. This dominant absorption band is typical of CO adsorbed on other conventional catalysts such as Pt/SiO_2 and Pt/Al_2O_3.[47,55,57]

As the concentration of the exchanging alkaline cation was increased by 10 mg/g increments, the band at 2070 cm^{-1} decreased in intensity and shifted to 2063 cm^{-1} meanwhile the bands at lower frequencies increased in intensity. The shoulder at 2105 cm^{-1} remained, and new bands appeared at 2082, 2063 and 2030 cm^{-1}. For Pt/KMFI (KX-10), the CO additional adsorption peaks were absent except for the peak centred at 2073 cm^{-1}, which indicates that the Pt environment in Pt/KMFI (KX-10) is different from that in the other catalysts.

It is noteworthy to compare the variations of the positions of the bands at 2063 cm^{-1} and 2030 cm^{-1} with increased K concentration. The continuous decrease in the intensity in the 2063 cm^{-1} peak and subsequent increase in the intensity in the peak at 2030 cm^{-1} is entirely attributed to K concentration. This high number of absorption bands reveals the presence of a variety of Pt

species. According to previous literature,[48,58] the band at 2030 cm^{-1} can be attributed to small Pt particles inside the zeolite channels while the accompanying band at 2063 cm^{-1} can be attributed to Pt particles on the outer zeolite surface, although this is not direct evidence of Pt particles inside the zeolite channels. The blue shift in the stretching vibration frequency of CO adsorbed on these particles results from the decrease of the electron density on the particles due to an interaction with strong Brønsted sites of highly acidic MFI zeolite **(Figure S11)**.[58,59] A concurrent shift in the centred adsorption peak is also suggestive of an attractive ion-dipole interaction whereby the basic promotor facilitates the chemisorption of CO on the Pt particles.[55,60] The marked redshift of the linear CO adsorption bands is attributed to an increase of electron density on these particles. An analogous effect is observed in alkaline and alkaline earth metal exchange Pt/BaL zeolite catalysts and Pt/Y zeolite catalysts whereby infrared bands corresponding to CO adsorption shifted up in frequency with increased acidity of the support.[61] It is also noteworthy that a change in the ratio of absorption bands attributed to small Pt particles in the zeolite channel (2030 cm^{-1}) and Pt particles on the outer zeolite surface (2060 cm^{-1}) was seen as as a function of Pt loading technique (IWI vs IE) (**Fig. 5d**). This is in agreement with STEM images observations of these two catalysts (**Figure S6**).

The bare supports did not adsorb CO and no absorption bands were observed in the spectral region 1750- 2150 cm^{-1}, confirming that the observed absorption bands in the Pt catalysts originate from CO adsorbed on Pt, not the support (**Figures S11-S14**).[62]

Pt/KMFI catalyst was further investigated via STEM (**Fig. 6a-d**). Pt particles are highly dispersed and have a narrow size distribution, indeed, Pt nanoparticles are <1 nm in diameter and no large (>5 nm) clusters were found on the catalyst. Isolated clusters of cationic Pt atoms on the channel wall are also observed. Pt nanoparticles are notably out of focus despite the electron beam being focussed on the top surface of the zeolite, furthermore, the b-axis of the MFI framework is clearly visible. These images indicate that Pt nanoparticles are inside the zeolite pores but not in the

straight channel along the b-axis, this observation is in agreement with our conclusions drawn from CO-DRIFTS analysis. Near identical observations are noted for Pt/KMFI (KX-40) (**Figure S15**). Crucially, in the absence of K, the spatial distribution and dispersion of Pt is greatly affected. STEM images of Pt/MFI clearly show large quantities of Pt clusters with >1 nm diameter on the outer surface of the zeolite and particularly undeseriable Pt agglomerates (>10 nm) are also seen (**Figure S16**). Furthermore, the Pt loading technique and heat treatment of Pt/KMFI and Pt/MFI were identical, highlighting the importance of K in dispersing and stabilizing Pt nanoparticles. Importantly, our STEM images mirror the observations of Liu et al. who, using STEM-iDPC techniques, have recevently demonstrated the preferred localization of subnanometer Pt clusters in the sinusoidal channels of purely siliceous MFI, stabilized by K^+ species.[63] We propose the same effect in this system where Pt is localized predominantly inside the pores, evidenced by no agglomeration on the external surface of Pt/KMFI.

We therefore reasonably propose that through careful K addition at an optimum concentration it is possible to load and stabilize small (<1 nm) Pt species primarily within the MFI pores, resulting in superior catalytic performance.

Mechanistic pathways of n-alkane aromatization

The effect of support, Pt localization and oxidation state, and K on the C_6 ring closure and dealkylation selectivities of these catalysts have been shown in the previous sections. The involved surface reaction mechanism will be of great interest for next investigation. Based on previous works[41] and the knowledge that alkenes are undoubtedly intermediates when moving from n-alkanes to aromatic hydrocarbons under non-oxidative conditions; we move to study varying alkene species under the same reaction conditions as before. Straight-chain monoalkenes, straight-chain dienes, and cyclic monoalkenes at different chain lengths (C_6-C_8) are examined to elucidate the possible reactive intermediates. Given the elevated activity of these species compared to n-alkanes, the conversions of these alkene reactions were kept between

60% and 70% as opposed to n-alkane reactions where conversions were maintained between 20% and 30%. Otherwise, conditions were the same as before (400°C, 145 psig initial N_2, 30 min reaction time). An understanding of the reaction mechanism is focused on the optimized Pt/KMFI (KX-40) catalyst, whose characteristics for superior performance are shown in the work leading up to this section, with comparisons drawn against Pt/MFI for clarity.

Reaction pathways of terminal straight-chain monoalkenes over Pt/KMFI (KX-40) and Pt/MFI

1-hexene and 1-octene were tested to see the product distribution over Pt/MFI and Pt/KMFI (KX-40). This is displayed in terms of reaction type to more clearly demonstrate the different reaction pathways (**Figures S17-S18**). Significantly enhanced double bond isomerization selectivity is observed over Pt/KMFI (KX-40) for both alkene feedstocks at 81.6 % and 78.4 % for 1-hexene and 1-octene reactions respectively. Zaera and co-workers have reported the unique capability of Pt(111) surfaces to catalyse the isomerisation of *trans*-alkenes to the more unstable *cis*-isomers,[64] echoed by our present experimental observations. As Pt/KMFI (KX-40) has negligible acidity and Pt is of relatively low valency, we suggest terminal alkene isomerization by the π-allyl mechanism. Furthermore, this mechanism results in a net zero change of Pt oxidation, as seen in our system, which results in double bond isomerization of the terminal alkene by addition and β-hydride elimination, followed by 1,3-H shifts.[65-68] There is much conflict in the literature as to the nature of this mechanism and so the one proposed here is tentative.[69]

The more ‘chaotic’ selectivity seen over Pt/MFI is typical of acidic catalysts which promote side reactions such as cracking and oligomerization,[70] 47.2 % and 30.7 % respectively for 1-hexene, and 66.9 % and 15.2 % for 1-octene. Skeletal isomerization only occurs over the Pt/MFI catalyst, a process that is also facilitated by the presence of strong acid sites.[71] The reduced skeletal isomerization selectivity for 1-octene reactions compared to 1-hexene over Pt/MFI suggest that the larger molecule encounters spatial difficulties during skeletal isomerization.[72] The summary

for the reaction of terminal alkenes over Pt/KMFI (KX) is that the catalyst is incapable of aromatizing these species and that they are thus probably not intermediates for the reaction of interest, the aromatization of n-alkanes. Furthermore, despite spatial constraints within the pores, the cyclisation reaction does not proceed.

Reaction pathways of straight-chain isolated dienes over Pt/KMFI (KX40) and Pt/MFI

Both catalysts exhibit similar selectivity by reaction type over 1,5-hexadiene (**Figure S19**), resulting in large amounts of oligomerization products which have carbon number greater than that of the original reactant. Recalling that cyclic species with a carbon number higher than 6 for the 1,5 hexadiene reactions are considered as oligomerization products, it is necessary to show the composition of this fraction (**Figure S23**). This shows that of the oligomerization products for 1,5 hexadiene reactions, 84.6% can be attributed to cyclic species when Pt/KMFI (KX-40) is used, and 80.8% for the Pt/MFI catalyst; similar distributions. Brønsted acid sites are known to be preferable sites to catalyse cyclisation in such systems through carbenium ion chemistry,[73] concluding that dienes are precursors for cyclisation for bifunctional catalysts, as seen in our data. Aromatization does not occur when isolated dienes are employed, contrary to a conjugated diene (**Figure S24**), this confirms the suspected mechanism in the Pt/MFI system. However, for the monofunctional Pt/KMFI (KX-40) system, aromatics are still not observed in the product, regardless of the diene being conjugated or isolated. This indicates the occurrence, for n-alkane reactions over Pt/KMFI (KX-40), of a direct C_6 ring closure on Pt followed by subsequent C-H bond ruptures as the metallocycle is dehydrogenated to aromatics. This mechanism would not occur if the intermediates were straight chain alkenes such as those shown in this work: monoalkenes, isolated dienes, and conjugated dienes. The formation of higher carbon number cyclic species than that of the reactant for 1,5-hexadiene reactions (**Figures S19**) was explained by Joshi et. al, who demonstrated the significantly lower energy barrier required to cyclise C_8 dienes compared to that of C_6 dienes because of the more stable secondary carbenium transition

state compared to the primary carbocationic transition state seen for C_6 dienes.[74] This phenomenon also demonstrates the possibility of such reactions over monofunctional Pt sites. Regardless of the mechanism of diene cyclisation over Pt/KMFI (KX-40); straight-chain dienes are clearly not intermediates for the desired C_6 ring closure and aromatization of n-alkanes, whose mechanism is displayed in more detail hereafter.

Reaction pathways of cyclic monoalkenes over Pt/KMFI (KX-40) and Pt/MFI

It is widely acknowledged that skeletal isomerisation and oligomerization of cyclic alkenes such as cyclohexene occurs over acid sites as witnessed over the Pt/MFI catalyst here (**Figure S21**). However, our Pt/KMFI (KX-40) system shows significant amounts of cyclic isomers when cyclohexene is reacted,with 28% selectivity towards methyl cyclopentene (**Figure S22**). This interesting reactivity suggests that the rings are opened and undergo C_5 ring closure to form these species. Flaherty et al. demonstrated with vibrational spectra and DFT calculations that sp^2 hybridised carbons in cycloalkanes bind to metals at temperatures >500 K (our system operates at 673.15 K) followed by C-C bond cleavage.[75] This explains the unexpected ring-opening observed over Pt/KMFI (KX-40) for cyclohexene and methylcyclohexene reactions. To further support this experimentally, we show that the reaction of cyclohexane over the monofunctional catalyst results in an almost pure benzene product, 97%, (**Table S3**), indicating that the absence of sp^2 hybridised carbons does not allow the C-C bond cleavage to occur. Bifunctional Pt/MFI yields a characteristic distribution of oligomerization products for all alkene feeds whilst low selectivity towards aromatic products is noted over Pt/KMFI (KX40) (**Figures S17-S24, Tables S8-S14**). Importantly, this is contrary to our observations with alkane feeds where Pt/KMFI (KX40) yields almost exclusively direct C_6-ring closure aromatics. Our data therefore strongly indicates that free alkene species are not involved as intermediates in the formation of C_6-ring closure products over Pt/KMFI (KX40).

Assement of intermediates and the positive influence of microporosity

Intermediate species were further assessed by conducting reactions at 4 different temperatures (300, 350, 375, and 400°C) and quenching immediately upon reaching those temperatures. This process was evaluated for Pt/MFI (**Fig. 7a**) and Pt/KMFI (KX-40) (**Fig. 7b**), with yields of the Pt/KMFI (KX-40) catalyst shown in **Fig. 7c**. These data indicate early isomerization of n-octane over Pt/KMFI (KX-40) at lower temperatures; isomerization is known to occur at lower temperatures,[76] even over metal sites.[77] Upon reaching 375°C, aromatization takes place and by 400°C, aromatization is the dominant reaction. These results support a direct C_6 ring closure mechanism over one active site with no desorption of intermediates, ie. The reaction occurs in a series of steps over the same active site. This one-step mechanism is also well documented and supported in the literature for supported non-acidic Pt catalysts.[16] A Pt on non-acidic γ-Al_2O_3 catalyst was prepared in an analogous manner to Pt/KMFI (KX-40). The textural properties of the catalyst were investigated by N_2 physisorption and n-octane aromatization performance was evaluated (**Table S2 and Figure S25**). The results demonstrate that external surface area is comparable and no micropores are present on Pt/γ-Al_2O_3. Given the change in total surface area, 0.5 wt% Pt was loaded to γ-Al_2O_3 to ensure a fair comparison. These data show n-octane isomerization occurs over the Pt/γ-Al_2O_3 catalyst, highlighting the importance of microporosity and shape selectivity for direct C_6 ring closure and inhibition of n-octane isomerization. It should be noted that C_6 ring closure does not occur solely within the micropores, evidenced by a significant amount of C_6 ring closure products over Pt/γ-Al_2O_3, in agreement with the literature.[78] These data suggest that the micropores of Pt/KMFI (KX-40) are vital to providing the necessary steric hinderance to maximize ring closure products and to avoid formation of straight-chain alkane isomers.

The complete mechanism for n-alkane aromatization over Pt/KMFI (KX)

By combining the observations made here we can conclude that the C_6 ring closure mechanism for n-alkanes (n-octane is given here as an example) occurs through the following mechanism over Pt/KMFI (KX-40) (**Fig. 8**): The terminal methyl of n-octane approaches Pt cluster to which the sp^3 hybridised carbon binds, steric hinderance of the inner pore forces the opposite terminal methyl group towards the same Pt cluster. However, formation of a C_8 metallocycle is unfavourable compared to the most stable C_6 metallocycle, assisted by puckering. 2,7 ring closure can also occur, to a lesser extent as the C_2 in n-octane, although less likely to bond to the Pt cluster than terminal methyls, is still preferable over other carbons. The resulting C_6 bimetallocycle, formed over Pt nanoparticles undergoes subsequent dehydrogenation to form a bimetallo-ethylcyclohexene followed by bimetallo-ethylcyclohexadiene and finally a bimetallo-ethylcyclohexatriene. Note that all these steps occur on the same site and no desorption and readsorption is thought to occur due to the absence of cyclopentenes in the product, which would form if the ethylcyclohexene were to desorb and readsorb as shown in the previous subsection. Furthermore, the absence of free intermediates in the product stream of low temperature reactions strengthens this hypothesis. Finally, the species becomes unbound from the Pt cluster to give the final product, ethylbenzene, or o-xylene if 2,7 ring closure has occurred. We reiterate that there are thought to be no gas phase intermediates during this process and that the aromatization of n-alkanes likely occurs over the same Pt nanoparticles for the duration of the reaction. However, a detailed kinetic investigation outside of the scope of the current work would be required to confidently confirm the reaction pathway of n-octane aromatization over Pt/KMFI (KX-40). The role of excess K as demonstrated in the previous sections of this work is proposed to ensure complete removal of acid sites, affect the support to create a stronger Pt support interaction, and to aid dispersion of Pt clusters. Our proposed mechanism and experimental data agree with the work of Somorjai and co-workers, who concluded that in the absence of excess hydrogen, hexane undergoes direct 1,6 ring closure over Pt (111) surfaces.[79] Furthermore, the authors provide spectroscopic evidence that the mechanism first proceeds through a π-allyl type

cyclohexane intermediate followed by irreversible dehydrogenation steps yielding benzene as the final product. The observed presence of dealkylation products is reasoned due to larger Pt clusters located primarily on the outer surface of the zeolite i.e. not within the pores. It is known that Pt nanoparticles loaded on non-acidic supports are capable of catalysing a variety of reactions when n-alkane feed is introduced, even in the absence of a porous structure such as that of zeolite LTL or MFI.[80] However, the presence of unwanted by-products such as alkenes, benzene and i-alkane isomerisation products are still noted, even over our optimized Pt/KMFI (KX-40) catalyst. Notably, selectivity towards such dealkylation products decreases with improved Pt dispersion and spatial distribution (**Fig. 3**). We therefore reasonably propose that, for Pt/KMFI catalysts, direct 1,6-direct ring closure occurs over small (<2 nm) nano clusters located primarily within the channels of MFI. Dealkylation is thought to be promoted by larger Pt clusters (>2 nm) which are primarily located on the external zeolite surface i.e. outside the pores.

Conclusions

We have reported the application of an MFI support loaded with K in excess beyond the IE limit and loaded with Pt by IWI for direct n-alkane aromatization through C_6 ring closure. This catalyst exhibited a high C_6 ring closure selectivity for n-octane, 86% compared to 27% over Pt/KL under equivalent conditions. The level of dealkylation was also reduced from 45% to 11% and is directly related to the level of carbon deposition inside the pores. This activity is attributed predominantly to the pore morphology where the lack of cages and single channels prevent heavy coking inside the pores, inhibit pore blocking, and promote easy diffusion of the C_6 ring closure products back to the gas phase during reaction. By adding potassium in excess beyond the IE limit; strong acidity is completely reduced, electron density of Pt particles is increased due to improved SMSI, and the dispersion of active Pt clusters is increased. Furthermore, Pt localization in the sinusoidal channels of MFI is strongly indicated by STEM. All these factors aid in promoting the desired C_6 ring closure mechanism for n-heptane and n-octane, in turn, eliminating inactive coke formation

and significantly enhancing catalyst lifetime. The mechanism for the acidic Pt/MFI and perfected Pt/KMFI (KX-40) systems is briefly considered and supported in the literature to further understanding of the C_6 ring closure mechanism through a bimetallocycle. This work highlights the effective use of a more economically favourable support for the highly selective aromatization of n-alkanes, increasing the potential for chemical feedstock production from the petrochemical industry as opposed to fuel improvement.

Methods

Synthesis of MFI support. MFI was synthesized hydrothermally where aluminium nitrate nonahydrate, 98% (Alfa Aesar) was added to tetra-propylammonium hydroxide, 40% wt. (Alfa Aesar) and stirred at RT until complete dissolution (approx. 10 mins). Tetraethyl orthosilicate (Merck KGaA) was added dropwise under the same stirring and temperature conditions. Post complete addition of tetraethyl orthosilicate it took approx. 1 h for supersaturation to occur. The gel was applied to a PTFE-lined autoclave and treated in a convection oven at 170°C for 72 h. Precursors were applied to achieve a molar ratio of Al_2O_3:30SiO_2:21TPAOH:943H_2O with the addition of excess DI water during the aluminium nitrate nonahydrate dissolution step if necessary. After removal from the oven, the crystals were washed 3 x in DI water by centrifugation to remove most of the remaining organics. The material was then applied to a convection oven at 80°C for 12 h and calcined in a continuous flow of air (200 SCCM) by heating at a rate of 5°C/min to 600°C and held for 3 hours. The result is MFI micrometric barrels approximately 150 nm in diameter.

Synthesis of KMFI. IE was conducted by addition of 10 g of support per 100 mL of 1.0 M KNO_3 (Alfa Aesar) which was stirred for 12 h at 70°C. The catalyst was then washed by centrifugation 3 times. The IE process was repeated twice more, the support was dried, and then calcined at 0.5°C/min to 600°C.

Synthesis of KMFI (KX). KCl was dissolved along with the Al precursor and TPAOH during the synthesis of MFI support to achieve desired $mg_K/g_{catalyst}$.

Pt loading onto KMFI. The support, as obtained above, was subjected to a 6.9 psi vacuum at 80°C for 6 h to ensure complete removal of water from the pores. Tetraammineplatinum (II) nitrate (Sigma Aldrich) was used as the Pt source. Pt was applied by incipient wetness impregnation (IWI) to maximize Pt localization in the pores as opposed to the external surface; physical trials showed saturation of the pores at 0.73 mL/g catalyst. 2.16 mL of 0.0711 M Pt metal solution was added in a dropwise manner to 2.97 g of support with vortex shaking followed by 12 h at 80°C under a 6.9 psi vacuum. The Pt loaded support was then applied to a continuous flow of air (200 SCCM) and heated at 0.5°C/min to 450°C and held for 2 h. After cooling to RT, a pure H_2 flow (200 SCCM) was applied and the sample heated at 5°C/min to 600°C and held for 2 h. This yielded Pt/KMFI. Pt/KL was synthesized in the same manner but the support (KL) was obtained commercially from Tosoh. All catalysts were synthesized for 1 % wt. nominal loading of Pt.

Experimental procedure and calculations. In a typical experiment, catalyst was loaded to a 300 mL Parr batch reactor system with 5 g of n-octane (98% from Sigma Aldrich). The catalyst mass was altered following subsequent experiments to achieve conversions between 20-30% for n-alkane reactions and 60-70% for alkene reactions. The reactor was then pressurised to 145 psig with pure N_2 (Air Liquide). The system was then heated at a rate of 20°C/min until 400°C where the temperature was held for 30 mins. Upon completion, the system was cooled naturally. The liquid product was extracted with 10 mL CS_2 (Sigma Aldrich) followed by a further dilution of a 0.5 mL aliquot in 10 mL CS_2. 0.5 mL of resulting solution was injected into a carefully calibrated gas chromatography-mass spectrometer (Perkin Elmer). The GC-MS (GC Claus 680 and MS Clarus SQ 8T) is equipped with a paraffin/olefin/naphthene/aromatic (PONA) column from Agilent. Gas products were analysed using a micro-GC (Agilent Technologies) with 4 columns: A 10m molecular sieve 5A, 10-m alumina, 8-m CP-Sil 5 CB, and a 10-m PPU. All columns are

equipped with thermal conductivity detectors. Calculation of selectivity was made on a weight % basis and was calculated according to equation (1).

(1)

Conversions were calculated according to equation (2).

(2)

TOF and productivity were calculated as per equations (3) and (4) respectively.

(3)

(4)

XRD Characterisation. XRD images were procured using a Rigaku Multiflex Diffractometer with Cu Kα irradiation at 20 kV and 40 mA in the 2θ region between 3° and 60°.

XANES Spectra. XANES spectra were obtained with an SM beamline (10ID-1) at the Canadian Light Source (CLS), which is equipped with a 35 nm outermost-zone plate (CXRO, Berkeley Lab). The diffraction-limited spatial resolution for the zone plate is 30 nm. Image sequence (stack) scans over a range of photon energies were acquired for the same sample region at the potassium K-edge.

N_2 physisorption analysis. N_2 isotherms were collected on a Micromeritics 3Flex. Samples (ca. 0.050 g) were degassed (150 °C, 6 h) prior to analysis. Analyses were carried out at 77 K with P_0 measured continuously. Free space was measured post- analysis with He. Pore size analysis was carried out using Micromeritics 3Flex software, N_2-Cylindrical Pores- Oxide Surface Model.

NH_3-TPD analysis. NH_3-TPD was carried out using a CHEMBET TPR/TPD chemisorption analyser, Quantachrome Industries fitted with a TCD. 50 mg of sample was pre-treated for 1 h at

130 °C (15 °C min^{-1}) in a flow of helium (80 mL min^{-1}). The sample was then cooled to ambient temperature and ammonia flowed through for 20 min to ensure saturation. The system was then heated 1 h at 100 °C (15 °C min^{-1}) under a flow of helium (80 mL min^{-1}) to remove physisorbed ammonia. Subsequently, chemisorbed ammonia was desorbed by heating to 900 °C (15 °C min^{-1}) in a flow of helium (80 mL min^{-1}) during which period desorbed ammonia was monitored using a TCD, current 180 mV, attenuation 1.

H_2 chemisorption analysis. H_2-TPR was conducted on a Finesorb-3010 chemisorption analyser by placement of 0.2 g catalyst sample in a quartz tubular chamber. The sample was initially purged in pure Ar and then oxidised in a 5% O_2 balance Ar gas mixture, heated at a rate of 10°C/min until 600°C and held for 30 mins. The Sample was then cooled to RT and placed in a 5% H_2 balance Ar gas flow where it was then heated at 10°C/min to 700°C/min and then instantly left to cool upon reaching the maximum temperature. A thermal conductivity detector (TCD) was used.

ICP-OES analysis. ICP-OES was conducted on an iCAP 7200 (Thermo Fisher Scientific) in Radial mode equipped with the Icap 7000 Radial HF kit and N_2 purge gas. In a typical sample pre-digestion, 0.5 g of sample was placed in a Teflon-lined autoclave capable of withstanding pressures up to 1500 psi. The sample was then digested by addition of 1 mL HF (Fisher Chemical, trace metal grade, 47-51%), 1 mL HNO_3 (VWR Aristar* Plus, for trace metal analysis, 67-70%), and 3 mL HCl (VWR Aristar* Plus for trace metal analysis, 34-37%) and placed in a convection oven overnight. The autoclave was removed and allowed to cool naturally. Samples were then diluted as aliquots in 2% HNO_3 and directly analysed by ICP-OES.

STEM imaging. Scanning transmission electron microscopy (STEM) was carried out in the National University of Singapore, using a JEOL ARM200F microscope with a cold Field Emission Source operated at 200kV. The STEM specimen was prepared by dry-disperse catalyst particles onto a holey carbon TEM copper grid.

TGA analysis. Thermogravimetric analysis (TGA) was conducted on a PerkinElmer STA 6000 simultaneous thermal analyser. Samples were ramped from 30°C to 800°C at a rate of 10°C/min in air.

XPS Analysis. X-ray photoelectron spectroscopy (XPS) measurements were performed using a Kratos Axis Ultra DLD photoelectron spectrometer using monochromatic Al k radiation (h = 1486.6 eV) operating at 120 W (10 mA x 12 kV). Samples were mounted on doubled sided adhesive tape decured on a glass slide attached to the spectromter sample holder. Data was acquired using pass enregies of 20 (0.1 eV step size) and 160 eV (1 eV step size) for high resolution and survey spectra repsectivley, using the 'Hybrid' mode of operation with a 'Slot' aperture which uses a combination of electrostatic and magnetic lens to enhance signal collection over a rectangular area of approximately 700 x 300 m. Data analysis, including charge refereincing to the adventious carbon C(1s) peak at 284.8 eV, was performed using CasaXPS (v2.3.23). Quantification was made after removal of a Shirley type background and modified Wagner sensitivity factors as supplied by the manufacturer.

CO-DRIFTS analysis. DRIFTS measurements were recorded from 1000 – 4000 cm^{-1} at a spectral resolution of 4 cm^{-1} (number of scans, 64) on a Bruker Tensor 27 spectrometer fitted with a mercury cadmium telluride (MCT) detector cooled by liquid N_2. A sample was loaded into the Praying Mantis high-temperature (HVC-DRP-4) in situ cell before exposure to N_2 and then 1% CO/N_2 at a flow rate of 20 cm^3 min^{-1}. A background spectrum was obtained using KBr, and measurements were recorded every 1 min at room temperature. Once the CO adsorption bands in the DRIFT spectra ceased to increase in intensity, the gas feed was changed back to N_2 and measurements were repeated until no change in subsequent spectra was observed.

Supporting Information

Supporting material and additional notes (Figures S1-S25; Tables S1-S14; Notes S1-S4)

Acknowledgments

We would like to thank the Canadian Light Source, where the XAS study described in the Supplementary Information of this paper was performed. The Canadian Light Source is supported by the Canada Foundation for Innovation, Natural Sciences and Engineering Research Council of Canada, the University of Saskatchewan, the Government of Saskatchewan, Western Economic Diversification Canada, the National Research Council Canada, and the Canadian Institutes of Health Research. Qian He would like to acknowledge the support by National Research Foundation (NRF) Singapore, under its NRF Fellowship (NRFF11-2019-0051).

References

(1) Thivasasith, A.; Maihom, T.; Pengpanich, S.; Limtrakul, J.; Wattanakit, C. Insights into the Reaction Mechanism of n-Hexane Dehydroaromatization to Benzene over Gallium Embedded HZSM-5: Effect of H_2 Incorporated on Active Sites*. Phys. Chem. Chem. Phys.* **2019**, *21*, 5359– 5367.

(2) Ahuja, R.; Punji, B.; Findlater, M.; Supplee, C.; Schinski, W.; Brookhart, M.; Goldman, A. S. Catalytic Dehydroaromatization of N-Alkanes by Pincer-Ligated Iridium Complexes. *Nat. Chem.* **2011**, *3*, 167–171.

(3) Musselwhite, N.; Na, K.; Alayoglu, S.; Somorjai, G. A. The Pathway to Total Isomer Selectivity: n-Hexane Conversion (Reforming) on Platinum Nanoparticles Supported on Aluminum Modified Mesoporous Silica (MCF-17). *J. Am. Chem. Soc.* **2014**, *136*, 16661–16665.

(4) Li, J.; He, Y.; Tan, L.; Zhang, P.; Peng, X.; Oruganti, A.; Yang, G.; Abe, H.; Wang, Y.; Tsubaki, N. Integrated Tuneable Synthesis of Liquid Fuels via Fischer–Tropsch Technology. *Nat. Catal.* **2018**, *1*, 787–793.

(5) Lane, G. S.; Modica, F. S.; Miller, J. T. Platinum/Zeolite Catalyst for Reforming n-Hexane: Kinetic and Mechanistic Considerations. *J. Catal.* **1991**, *129*, 145–158.

(6) Manninger, I.; Xu; Lun, X.; Tétényi, P.; Paál, Z. Aromatization of n-Hexane over Pt-KL Catalyst. *Appl. Catal.* **1989**, *51*, L7–L11.

(7) Davis, R. J.; Derouane, E. G. A Non-Porous Supported-Platinum Catalyst for Aromatization of n-Hexane. *Nature* **1991**, *349*, 313–315.

(8) Xu, D.; Wang, S.; Wu, B.; Zhang, B.; Qin, Y.; Huo, C.; Huang, L.; Wen, X.; Yang, Y.; Li, Y. Highly Dispersed Single-Atom Pt and Pt Clusters in the Fe-Modified KL Zeolite with Enhanced Selectivity for n-Heptane Aromatization. *ACS Appl. Mater. Interfaces* **2019**, *11*, 29858–29867.

(9) Bernard, J. R. Proceedings of the Fifth International Conference on Zeolites. *Proceedings of the Fifth International Conference on Zeolites* **1980**, 686–695.

(10) Mielczarski, E.; Hong, S. B.; Davis, R. J.; Davis, M. E. Aromatization of n-Hexane by Platinum-Containing Molecular Sieves II. n-Hexane Reactivity. *J. Catal.* **1992**, *134*, 359–369.

(11) Derouane, E. G.; Vanderveken, D. J. Structural Recognition and Preorganization in Zeolite Catalysis: Direct Aromatization of n-Hexane on Zeolite L-Based Catalysts. *Appl. Catal.* **1988**, *45*, L15–L22.

(12) Miller, J. T.; Agrawal, N. G. B.; Lane, G. S.; Modica, F. S. Effect of Pore Geometry on Ring Closure Selectivities in Platinum L-Zeolite Dehydrocyclization Catalysts. *J. Catal.* **1996**, *163*, 106– 116.

(13) Azzam, K. G.; Jacobs, G.; Shafer, W. D.; Davis, B. H. Aromatization of Hexane over Pt/KL Catalyst: Role of Intracrystalline Diffusion on Catalyst Performance Using Isotope Labeling. *J. Catal.* **2010**, *270*, 242–248.

(14) Lee, K.; Choi, M. Hierarchically Micro-/Mesoporous Pt/KL for Alkane Aromatization: Synergistic Combination of High Catalytic Activity and Suppressed Hydrogenolysis. *J. Catal.* **2016**, *340*, 66–75.

(15) Jentoft, R. E.; Tsapatsis, M.; Davis, M. E.; Gates, B. C. Platinum Clusters Supported in Zeolite LTL: Influence of Catalyst Morphology on Performance in n-Hexane Reforming. *J. Catal.* **1998**, *179*, 565–580.

(16) Mériaudeau, P.; Naccache, C.; Meriaudeau, P. Dehydrocyclization of Alkanes Over Zeolite-Supported Metal Catalysts: Monofunctional or Bifunctional Route. *Catal. Rev.* **1997**, *39*, 5–48.

(17) Dai, L.-X.; Sakashita, H.; Tatsumi, T. Studies on the Surface Property of Pt/KL Zeolite Catalysts. *Bull. Chem. Soc. Jpn.* **1994**, *67*, 1553–1559.

(18) McVicker, G. B.; Kao, J. L.; Ziemiak, J. J.; Gates, W. E.; Robbins, J. L.; Treacy, M. M. J.; Rice, S. B.; Vanderspurt, T. H.; Cross, V. R.; Ghosh, A. K. Effect of Sulfur on the Performance and on the Particle Size and Location of Platinum in Pt/KL Hexane Aromatization Catalysts. *J. Catal.* **1993**, *139*, 48–61.

(19) Xu, D.; Wang, S.; Wu, B.; Huo, C.; Qin, Y.; Zhang, B.; Yin, J.; Huang, L.; Wen, X.; Yang, Y.; Li, Y. Tailoring Pt Locations in KL Zeolite by Improved Atomic Layer Deposition for Excellent Performance in n-Heptane Aromatization. *J. Catal.* **2018**, *365*, 163–173.

(20) Besoukhanova, C.; Guidot, J.; Barthomeuf, D.; Breysse, M.; Bernard, J. R. Platinum-Zeolite Interactions in Alkaline L Zeolites. Correlations Between Catalytic Activity and Platinum State. *J. Chem. Soc. Faraday Trans. 1 Phys. Chem. Condens. Phases* **1981**, *77*, 1595–1604.

(21) Li, K.; Chang, Q.; Yin, J.; Zhao, C.; Huang, L.; Tao, Z.; Yun, Y.; Zhang, C.; Xiang, H.; Yang, Y.; Li, Y. Deactivation of Pt/KL Catalyst during n-Heptane Aromatization Reaction. *J. Catal.* **2018**, *361*, 193–203.

(22) Zhao, C.; Wu, B.; Tao, Z.; Li, K.; Li, T.; Gao, X.; Huang, L.; Yun, Y.; Yang, Y.; Li, Y. Synthesis of Nano-Sized LTL Zeolite by Addition of a Ba Precursor with Superior n-Octane Aromatization Performance. *Catal. Sci. Technol.* **2018**, *8*, 2860–2869.

(23) Jongpatiwut, S.; Sackamduang, P.; Rirksomboon, T.; Osuwan, S.; Resasco, D. E. n-Octane Aromatization on a Pt/KL Catalyst Prepared by Vapor-Phase Impregnation. *J. Catal.* **2003**, *218*, 1–11.

(24) Najafpoor, A. A.; Jonidi Jafari, A.; Hosseinzadeh, A.; Khani Jazani, R.; Bargozin, H. Optimization of Non-Thermal Plasma Efficiency in the Simultaneous Elimination of Benzene, Toluene, Ethyl-Benzene, and Xylene from Polluted Airstreams Using Response Surface Methodology. *Environ. Sci. Pollut. Res.* **2018**, *25*, 233–241.

(25) Trakarnroek, S.; Ittisanronnachai, S.; Jongpatiwut, S.; Rirksomboon, T.; Osuwan, S.; Resasco, D. E. Effect of Zeolite Crystallite Size on Pt/KL Catalysts Used for the Aromatization of n-Octane. *Chem. Eng. Commun.* **2007**, *194*, 946–961.

(26) Benito, P. L.; Gayubo, A. G.; Aguayo, A. T.; Olazar, M.; Bilbao, J. Deposition and Characteristics of Coke over a H-ZSM5 Zeolite-Based Catalyst in the MTG Process. *Ind. Eng. Chem. Res.* **1996**, *35*, 3991–3998.

(27) Huang, J.; Jiang, Y.; Marthala, V. R. R.; Bressel, A.; Frey, J.; Hunger, M. Effect of Pore Size and Acidity on the Coke Formation during Ethylbenzene Conversion on Zeolite Catalysts. *J. Catal.* **2009**, *263*, 277–283.

(28) Meng, Y.; Genuino, H. C.; Kuo, C. H.; Huang, H.; Chen, S. Y.; Zhang, L.; Rossi, A.; Suib, S. L. One-Step Hydrothermal Synthesis of Manganese-Containing MFI-Type Zeolite, Mn-ZSM-5, Characterization, and Catalytic Oxidation of Hydrocarbons. *J. Am. Chem. Soc.* **2013**, *135*, 8594– 8605.

(29) Kukla, V.; Kornatowski, J.; Demuth, D.; Girnus, I.; Pfeifer, H.; Rees, L. V. C.; Schunk, S.; Unger, K. K.; Kärger, J. NMR Studies of Single-File Diffusion in Unidimensional Channel Zeolites. *Science* **1996**, *272*, 702–704.

(30) Palumbo, L.; Bonino, F.; Beato, P.; Bjørgen, M.; Zecchina, A.; Bordiga, S. Conversion of Methanol to Hydrocarbons: Spectroscopic Characterization of Carbonaceous Species Formed over H-ZSM-5. *J. Phys. Chem. C* **2008**, *112*, 9710–9716.

(31) Bjørgen, M.; Svelle, S.; Joensen, F.; Nerlov, J.; Kolboe, S.; Bonino, F.; Palumbo, L.; Bordiga, S.; Olsbye, U. Conversion of Methanol to Hydrocarbons over Zeolite H-ZSM-5: On the Origin of the Olefinic Species. *J. Catal.* **2007**, *249*, 195–207.

(32) Silva, J. M.; Ribeiro, M. F.; Ribeiro, F. R.ˆa; Benazzi, E.; Guisnet, M. Transformation of an Ethylbenzene-o-Xylene Mixture on HMOR and Pt-HMOR Catalysts. Comparison with ZSM-5 Catalysts. *Appl. Catal. A Gen.* **1995**, *125*, 15–27.

(33) Li, Y.; Zhang, C.; Liu, Y.; Tang, S.; Chen, G.; Zhang, R.; Tang, X. Coke Formation on the Surface of Ni/HZSM-5 and Ni-Cu/HZSM-5 Catalysts during Bio-Oil Hydrodeoxygenation. *Fuel* **2017**, *189*, 23–31.

(34) De Graaf, J.; Van Dillen, A. J.; De Jong, K. P.; Koningsberger, D. C. Preparation of Highly Dispersed Pt Particles in Zeolite Y with a Narrow Particle Size Distribution: Characterization by Hydrogen Chemisorption, TEM, EXAFS Spectroscopy, and Particle Modeling. *J. Catal.* **2001**, *203*, 307–321.

(35) Rubio-Marqués, P.; Rivero-Crespo, M. A.; Leyva-Pérez, A.; Corma, A. Well-Defined Noble Metal Single Sites in Zeolites as an Alternative to Catalysis by Insoluble Metal Salts. *J. Am. Chem. Soc.* **2015**, *137*, 11832–11837.

(36) Wang, Z.; Shen, X.; Yan, Y.; Qian, T.; Wang, J.; Sun, Q.; Jin, C. Facile Fabrication of a PDMS @ Stearic Acid-Al$(OH)_3$ Coating on Lignocellulose Composite with Superhydrophobicity and Flame Retardancy. *Appl. Surf. Sci.* **2018**, *450*, 387–395.

(37) Jackson, C.; Smith, G. T.; Inwood, D. W.; Leach, A. S.; Whalley, P. S.; Callisti, M.; Polcar, T.; Russell, A. E.; Levecque, P.; Kramer, D. Electronic Metal-Support Interaction Enhanced Oxygen Reduction Activity and Stability of Boron Carbide Supported Platinum. *Nat. Commun.* **2017**, *8*, 1–11.

(38) Matin, M. A.; Lee, E.; Kim, H.; Yoon, W. S.; Kwon, Y. U. Rational Syntheses of Core-Shell Fe@(PtRu) Nanoparticle Electrocatalysts for the Methanol Oxidation Reaction with Complete Suppression of CO-Poisoning and Highly Enhanced Activity. *J. Mater. Chem. A* **2015**, *3*, 17154– 17164.

(39) Costa, C.; Dzikh, I. P.; Lopes, J. M.; Lemos, F.; Ribeiro, F. R. Activity-Acidity Relationship in Zeolite ZSM-5. Application of Bronsted-Type Equations. *J. Mol. Catal. A Chem.* **2000**, *154*, 193-201.

(40) Schreiber, M. W.; Plaisance, C. P.; Baumgärtl, M.; Reuter, K.; Jentys, A.; Bermejo-Deval, R.; Lercher, J. A. Lewis-Brønsted Acid Pairs in Ga/H-ZSM-5 to Catalyze Dehydrogenation of Light Alkanes. *J. Am. Chem. Soc.* **2018**, *140*, 4849–4859.

(41) Harrhy, J. H.; Wang, A.; Jarvis, J. S.; He, P.; Meng, S.; Yung, M.; Liu, L.; Song, H. Understanding Zeolite Deactivation by Sulfur Poisoning during Direct Olefin Upgrading. *Commun. Chem.* **2019**, *2*, 1–13.

(42) Groen, J. C.; Bach, T.; Ziese, U.; Paulaime-Van Donk, A. M.; De Jong, K. P.; Moulijn, J. A.; Pérez-Ramírez, J. Creation of Hollow Zeolite Architectures by Controlled Desilication of A1-Zoned ZSM-5 Crystals. *J. Am. Chem. Soc.* **2005**, *127*, 10792–10793.

(43) Matsubu, J. C.; Zhang, S.; DeRita, L.; Marinkovic, N. S.; Chen, J. G.; Graham, G. W.; Pan, X.; Christopher, P. Adsorbate-Mediated Strong Metal-Support Interactions in Oxide-Supported Rh Catalysts. *Nat. Chem.* **2017**, *9*, 120–127.

(44) Tauster, S. J.; Fung, S. C.; Garten, R. L. Strong Metal-Support Interactions. Group 8 Noble Metals Supported on TiO_2. *J. Am. Chem. Soc.* **1978**, *100*, 170–175.

(45) Deng, L.; Miura, H.; Shishido, T.; Wang, Z.; Hosokawa, S.; Teramura, K.; Tanaka, T. Elucidating Strong Metal-Support Interactions in Pt–Sn/SiO_2 Catalyst and Its Consequences for Dehydrogenation of Lower Alkanes. *J. Catal.* **2018**, *365*, 277–291.

(46) Hsu, C. Y.; Chiu, T. C.; Shih, M. H.; Tsai, W. J.; Chen, W. Y.; Lin, C. H. Effect of Electron Density of Pt Catalysts Supported on Alkali Titanate Nanotubes in Cinnamaldehyde Hydrogenation. *J. Phys. Chem. C* **2010**, *114*, 4502–4510.

(47) Stakheev, A. Y.; Shpiro, E. S.; Jaeger, N. I.; Schulz-Ekloff, G. Electronic State and Location of Pt Metal Clusters in KL Zeolite: FTIR Study of CO Chemisorption. *Catal. Letters* **1995**, *32*, 147–158.

(48) Chakarova, K.; Mihaylov, M.; Hadjiivanov, K. FTIR Spectroscopic Study of CO Adsorption on Pt-H-ZSM-5. *Microporous Mesoporous Mater.* **2005**, *81*, 305–312.

(49) Primet, M.; Basset, J. M.; Mathieu, M. V.; Prettre, M. Infrared Study of CO Adsorbed on Pt Al_2O_3. A Method for Determining Metal-Adsorbate Interactions. *J. Catal.* **1973**, *29*, 213–223.

(50) Barth, R.; Pitchai, R.; Anderson, R. L.; Verykios, X. E. Thermal Desorption-Infrared Study of Carbon Monoxide Adsorption by Alumina-Supported Platinum. *J. Catal.* **1989**, *116*, 61–70.

(51) Jackson, S. D.; Glanville, B. M.; Willis, J.; McLellan, G. D.; Webb, G.; Moyes, R. B.; Simpson, S.; Wells, P. B.; Whyman, R. Supported Metal Catalysts: Preparation, Characterization, and Function: II. Carbon Monoxide and Dioxygen Adsorption on Platinum Catalysts. *J. Catal.* **1993**, *139*, 207–220.

(52) Ding, K.; Gulec, A.; Johnson, A. M.; Schweitzer, N. M.; Stucky, G. D.; Marks, L. D.; Stair, P. C. Identification of Active Sites in CO Oxidation and Water-Gas Shift over Supported Pt Catalysts. *Science* **2015**, *350*, 189–192.

(53) Jongpatiwut, S.; Sackamduang, P.; Rirksomboon, T.; Osuwan, S.; Alvarez, W. E.; Resasco, D. E. Sulfur- and Water-Tolerance of Pt/KL Aromatization Catalysts Promoted with Ce and Yb. *Appl. Catal. A Gen.* **2002**, *230*, 177–193.

(54) Yang, X.; Su, X.; Chen, X.; Duan, H.; Liang, B.; Liu, Q.; Liu, X.; Ren, Y.; Huang, Y.; Zhang, T. Promotion Effects of Potassium on the Activity and Selectivity of Pt/Zeolite Catalysts for Reverse Water Gas Shift Reaction. *Appl. Catal. B Environ.* **2017**, *216*, 95–105.

(55) Bourane, A.; Dulaurent, O.; Bianchi, D. Heats of Adsorption of the Linear CO Species Adsorbed on a Pt/Al2O3 Catalyst in the Presence of Coadsorbed Species Using FTIR Spectroscopy. *Langmuir* **2001**, *17*, 5496–5502.

(56) Han, W. J.; Kooh, A. B.; Hicks, R. F. Infrared Spectroscopy of Carbon Monoxide Adsorbed on Pt/L Zeolite. *Catal. Letters* **1993**, *18*, 193–208.

(57) Chafik, T.; Dulaurent, O.; Gass, J. L.; Bianchi, D. Heat of Adsorption of Carbon Monoxide on a Pt/Rh/CeO_2/Al_2O_3 Three-Way Catalyst Using in-Situ Infrared Spectroscopy at High Temperatures. *J. Catal.* **1998**, *179*, 503–514.

(58) Stakheev, A. Y.; Shpiro, E. S.; Tkachenko, O. P.; Jaeger, N. I.; Schulz-Ekloff, G. Evidence for Monatomic Platinum Species in H-ZSM-5 from FTIR Spectroscopy of Chemisorbed CO. *J. Catal.* **1997**, *169*, 382–388.

(59) Sachtler, W. M. H.; Stakheev, A. Y. Electron-Deficient Palladium Clusters and Bifunctional Sites in Zeolites. *Catal. Today* **1992**, *12*, 283–295.

(60) Visser, T.; Nijhuis, T. A.; Van Der Eerden, A. M. J.; Jenken, K.; Ji, Y.; Bras, W.; Nikitenko, S.; Ikeda, Y.; Lepage, M.; Weckhuysen, B. M. Promotion Effects in the Oxidation of CO over Zeolite-Supported Pt Nanoparticles. *J. Phys. Chem. B* **2005**, *109*, 3822–3831.

(61) Gallezot, P. The State and Catalytic Properties of Platinum and Palladium in Faujasite-Type Zeolites. *Catal. Rev.* **1979**, *20*, 121–154.

(62) Kubanek, P.; Schmidt, H. W.; Spliethoff, B.; Schüth, F. Parallel IR Spectroscopic Characterization of CO Chemisorption on Pt Loaded Zeolites. *Microporous Mesoporous Mater.* **2005**, *77*, 89–96.

(63) Liu, L.; Lopez-Haro, M.; Lopes, C. W.; Li, C.; Concepcion, P.; Simonelli, L.; Calvino, J. J.; Corma, A. Regioselective Generation and Reactivity Control of Subnanometric Platinum Clusters in Zeolites for High-Temperature Catalysis. *Nat. Mater.* **2019**, *18*, 866–873.

(64) Lee, I.; Zaera, F. Selectivity in Platinum-Catalyzed Cis-Trans Carbon-Carbon Double-Bond Isomerization. *J. Am. Chem. Soc.* **2005**, *127*, 12174–12175.

(65) Larionov, E.; Li, H.; Mazet, C. Well-Defined Transition Metal Hydrides in Catalytic Isomerizations. *Chem. Commun.* **2014**, *50*, 9816–9826.

(66) Knapp, S. M. M.; Shaner, S. E.; Kim, D.; Shopov, D. Y.; Tendler, J. A.; Pudalov, D. M.; Chianese, A. R. Mechanistic Studies of Alkene Isomerization Catalyzed by CCC-Pincer Complexes of Iridium. *Organometallics* **2014**, *33*, 473–484.

(67) Scarso, A.; Colladon, M.; Sgarbossa, P.; Santo, C.; Michelin, R. A.; Strukul, G. Highly Active and Selective Platinum(II)-Catalyzed Isomerization of Allylbenzenes: Efficient Access to (E)-Anethole and Other Fragrances via Unusual Agostic Intermediates. *Organometallics* **2010**, *29*, 1487–1497.

(68) Becica, J.; Glaze, O. D.; Wozniak, D. I.; Dobereiner, G. E. Selective Isomerization of Terminal Alkenes to (Z)-2-Alkenes Catalyzed by an Air-Stable Molybdenum(0) Complex. *Organometallics* **2018**, *37*, 482–490.

(69) Li, J.; Fleurat-Lessard, P.; Zaera, F.; Delbecq, F. Switch in Relative Stability between Cis and Trans 2-Butene on Pt(111) as a Function of Experimental Conditions: A Density Functional Theory Study. *ACS Catal.* **2018**, *8*, 3067–3075.

(70) Nash, R. J.; Dry, M. E.; O'Connor, C. T. Aromatization of 1-Hexene and 1-Octene by Gallium/H-ZSM-5 Catalysts. *Appl. Catal. A Gen.* **1996**, *134*, 285–297.

(71) Kazansky, V. B. The Nature of Adsorbed Carbenium Ions as Active Intermediates in Catalysis by Solid Acids. Acc. *Chem. Res.* **1991**, *24*, 379–383.

(72) Kim, W. G.; Kim, J. H.; Ahn, B. J.; Seo, G. The Skeletal Isomerization of C_4-C_7 1-Olefins over Ferrierite and ZSM-5 Zeolite Catalysts. *Korean J. Chem. Eng.* **2001**, *18*, 120–126.

(73) Joshi, Y. V.; Thomson, K. T. Embedded Cluster (QM/MM) Investigation of C_6 Diene Cyclization in HZSM-5. *J. Catal.* **2005**, *230*, 440–463.

(74) Joshi, Y. V.; Thomson, K. T. Brønsted Acid Catalyzed Cyclization of C_7 and C_8 Dienes in HZSM-5: A Hybrid QM/MM Study and Comparison with C_6 Diene Cyclization. *J. Phys. Chem. C* **2008**, *112*, 12825–12833.

(75) Flaherty, D. W.; Uzun, A.; Iglesia, E. Catalytic Ring Opening of Cycloalkanes on Ir Clusters: Alkyl Substitution Effects on the Structure and Stability of C-C Bond Cleavage Transition States. *J. Phys. Chem. C* **2015**, *119*, 2597–2613.

(76) Grau, J. M.; Benitez, V. M.; Yori, J. C.; Vera, C. R.; Padilha, J. F.; Magalhaes Pontes, L. A.; Silva, A. O. S. Isomerization Cracking of n-Octane and n-Decane on Regulated Acidity Pt/WOx-SO_4-ZrO_2 Catalysts. *Energy and Fuels* **2007**, *21*, 1390–1395.

(77) Naqvi, S. R.; Bibi, A.; Naqvi, M.; Noor, T.; Nizami, A.-S.; Rehan, M.; Ayoub, M. New Trends in Improving Gasoline Quality and Octane through Naphtha Isomerization: A Short Review. *Appl. Petrochemical Res.* **2018**, *8*, 131–139.

(78) Sivasanker, S.; Padalkar, S. R. Mechanism of Dehydrocyclization of n-Alkanes over Platinum-Alumina Catalysts. *Appl. Catal.* **1988**, *39*, 123–126.

(79) Yang, M.; Somorjai, G. A. Adsorption and Reactions of C_6 Hydrocarbons at High Pressures on Pt(111) Single-Crystal Surfaces Studied by Sum Frequency Generation Vibrational Spectroscopy: Mechanisms of Isomerization and Dehydrocyclization of n-Hexane. *J. Am. Chem. Soc.* **2004**, *126*, 7698–7708.

(80) Davis, B. H. Alkane Dehydrocyclization Mechanism. *Catal. Today* **1999**, *53*, 443–516.

Author information

Affiliations

Department of Chemical and Petroleum Engineering, University of Calgary, 2500 University Dr NW, Calgary, Alberta T2N 1N4, Canada

Jack S. Jarvis, Jonathan H. Harrhy, Aiguo Wang, Hua Song

Cardiff Catalysis Institute, Department School of Chemistry, Cardiff University, Main Building, Park Place, Cardiff, UK CF10 3AT.

Takudzwa Bere, James H. Carter, David J. Morgan, Graham J. Hutchings

Department of Materials Science and Engineering, National University of Singapore, 9 Engineering Drive 1, Block EA #03-09, 117575, Singapore

Qian He, Alexander G. R. Howe.

Contributions

J.S.J. and J.H.H. contributed to the experimental planning, experimental measurements, analysis of data, and manuscript preparation. A.W. conducted H_2 chemisorption and TGA analysis and provided guidance on interpretation. T.B. and J.H.C. performed and interpreted CO-DRIFTS analysis. D.J.M. performed and interpreted XPS analysis. Q.H. and A.G.R.H. carried out the STEM characterisation. G.J.H. and H.S. contributed to experimental planning, data analysis and manuscript preparation.

Corresponding author

Correspondence to Dr. Hua Song.

Ethics declarations

The authors have no competing interests to declare.

Figures

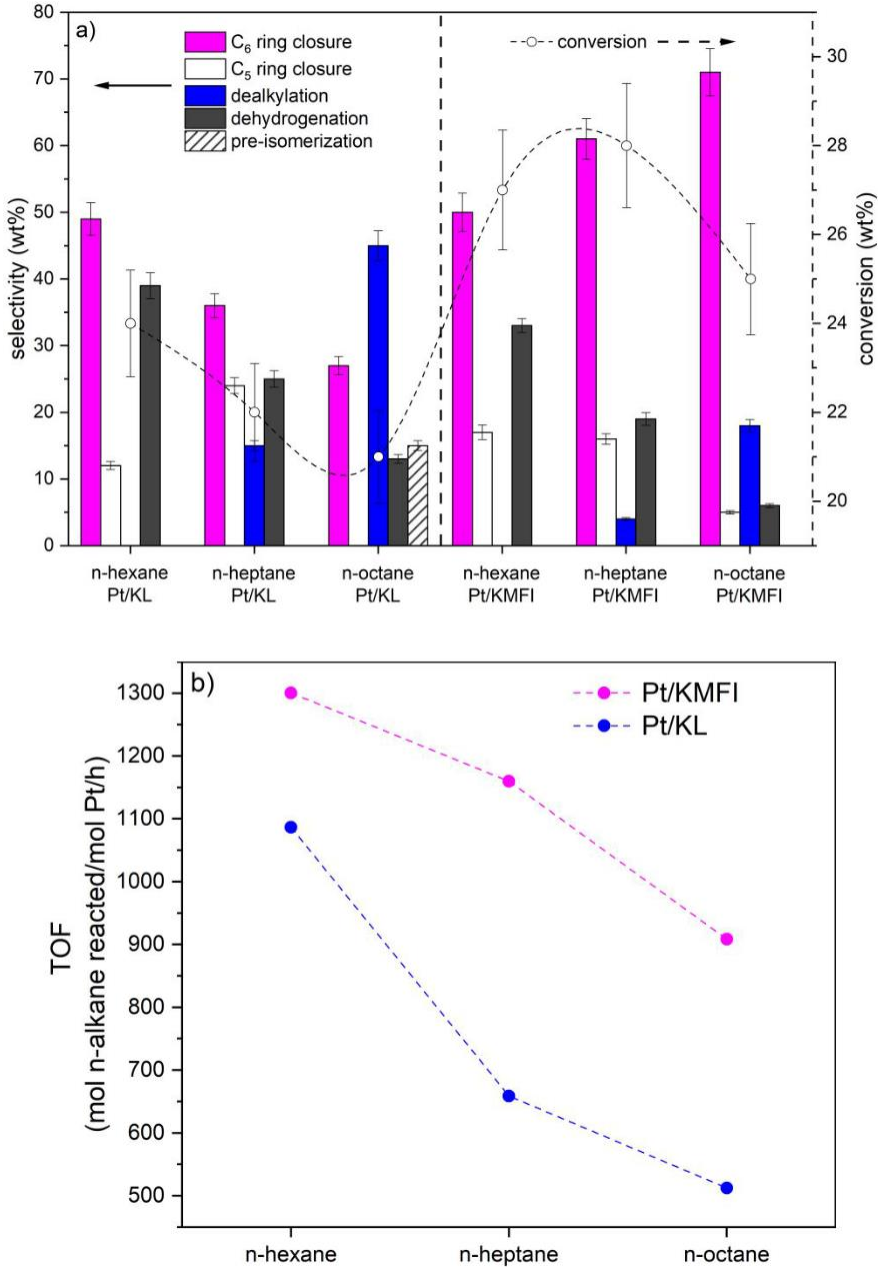

Fig. 1) Reactions of n-alkanes over Pt/KL and Pt/KMFI catalysts. *Reactions were conducted at 400°C and 145 psig initial N_2 for 30 mins. Conversions were maintained between 21% and 28% by altering the catalyst loading. C_6 ring closure (magenta) includes cycloalkanes yet to be aromatized and C_5 ring closure (white) refers to cyclopentane and cyclopentene type products. Dealkylation (blue) includes methane and aromatics resulting from the loss of one or two methyl*

groups. Dehydrogenation (dark grey) refers to alkenes. Pre-isomerisation (white with parallel dark grey stripes) refers to m- and p-xylenes which result from isomerisation of cyclic species followed by aromatization (a). Reaction performance shown as TOF to account for catalyst mass used in each reaction. Pt/KMFI (magenta) and Pt/KL (blue), where TOF is defined as moles of n-alkane reacted/mol Pt/h (b). Errors calculated as standard deviation as given as +/- 5%. This error analysis is carried through for all other relevant figures.

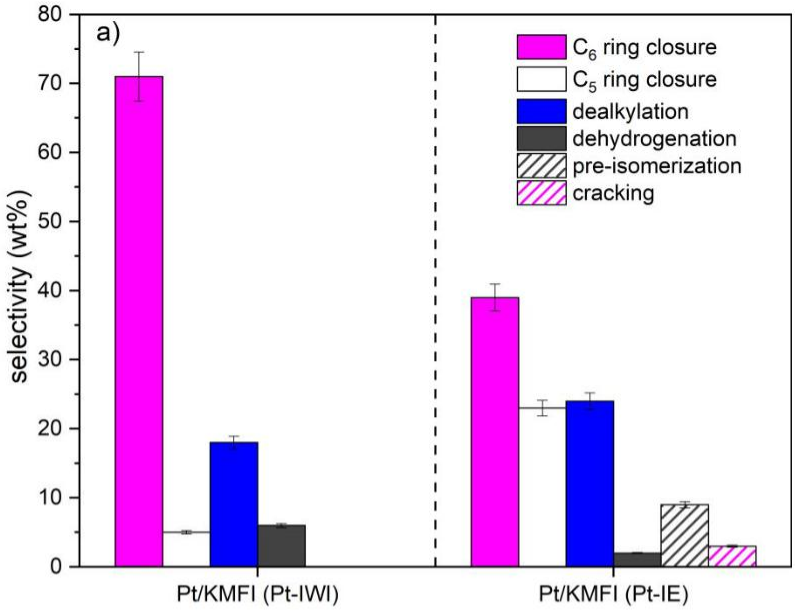

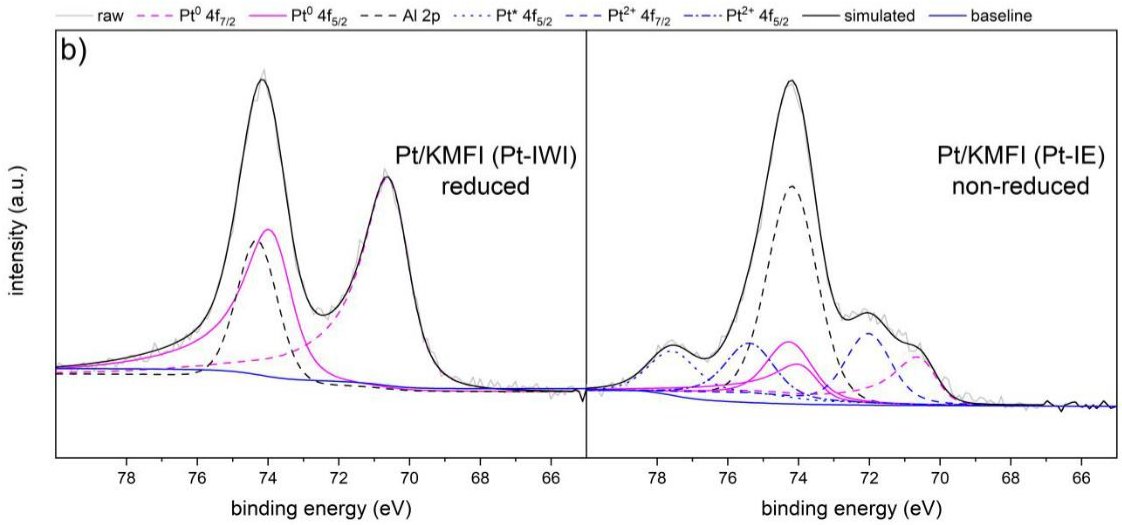

Fig. 2) Aromatization reaction performance of n-octane, and XPS spectra of the Al 2p and Pt 4f regions of Pt/KMFI (Pt-IWI) and Pt/KMFI (Pt-IE) catalysts. *Reactions of n-octane over Pt/KMFI (Pt-IWI) and Pt/KMFI (Pt-IE) catalysts (a). Reactions were conducted at 400°C and 145 psig initial N_2 for 30 mins. Conversions were 25% and 19% respectively. C_6 ring closure (magenta) includes cycloalkanes yet to be aromatized and C_5 ring closure (white) refers to cyclopentane and cyclopentene type products. Dealkylation (blue) includes methane and aromatics resulting from the loss of one or two methyl groups. Dehydrogenation (dark grey) refers to alkenes. Pre-isomerisation (white with parallel dark grey stripes) refers to m- and p-xylenes which result from isomerisation of cyclic species followed by aromatization. Cracking (white with parallel magenta stripes) represents all products <C_8 except for benzene, toluene, and methane. XPS spectra of the Al 2p and Pt 4f regions of Pt/KMFI (Pt-IWI) and Pt/KMFI (Pt-IE) catalysts (b).*

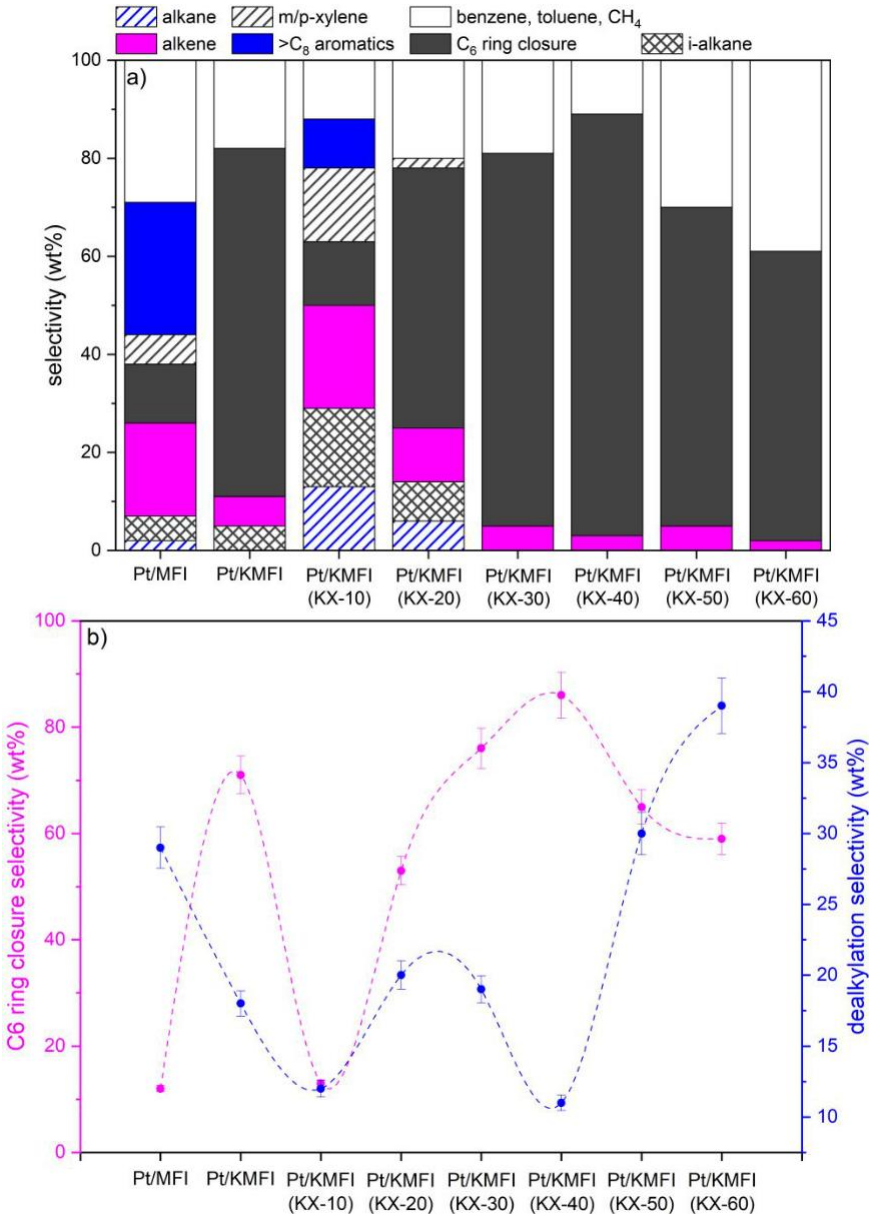
alkane
alkene
m/p-xylene
>C8 aromatics
benzene, toluene, CH4
C6 ring closure
i-alkane
a)
selectivity (wt%)
Pt/MFI
Pt/KMFI
Pt/KMFI (KX-10)
Pt/KMFI (KX-20)
Pt/KMFI (KX-30)
Pt/KMFI (KX-40)
Pt/KMFI (KX-50)
Pt/KMFI (KX-60)
b)
C6 ring closure selectivity (wt%)
dealkylation selectivity (wt%)

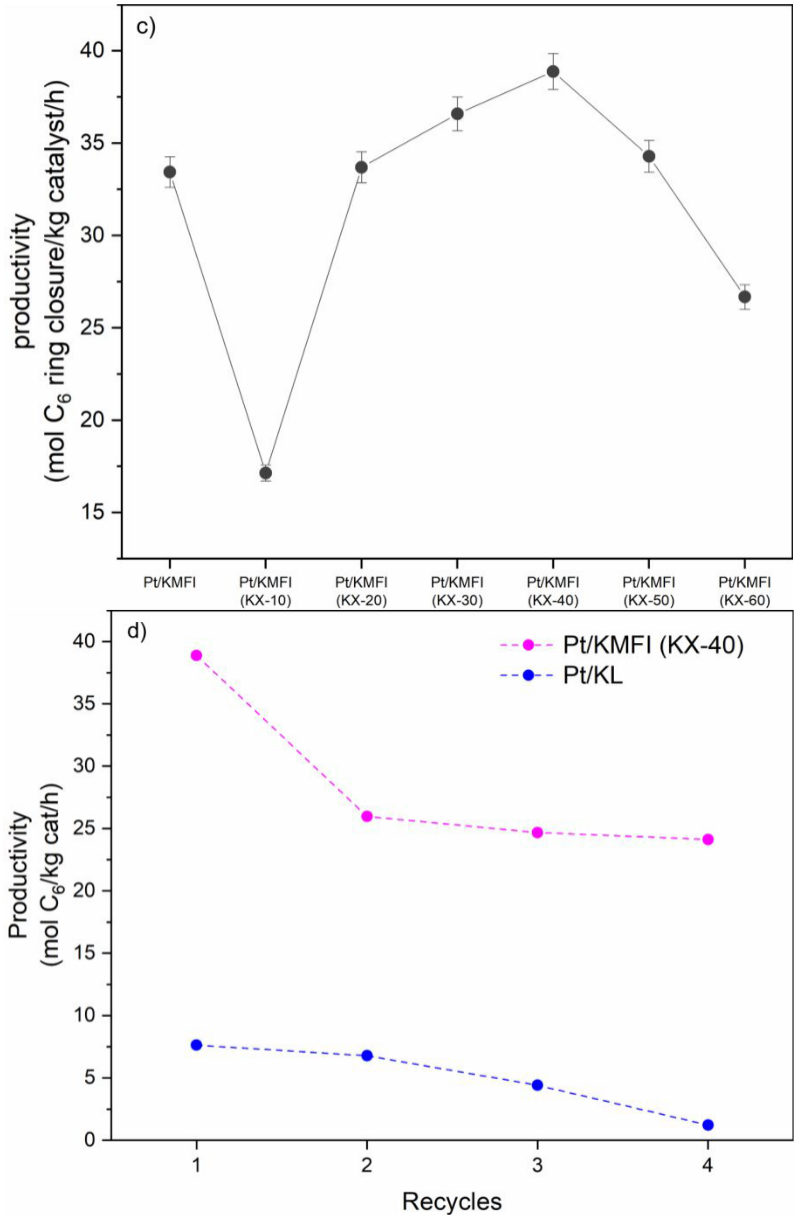

Fig. 3) Performance evaluation of n-octane aromatization reactions over Pt/KMFI (KX) at controlled excess potassium increments. *Reactions were conducted at 400°C and 145 psig initial N_2 for 30 mins. Conversions were maintained between 20 and 30% by altering the catalyst loading. Total selectivity, wt%, showing benzene, toluene, and CH_4 (white), >C_8 aromatics (blue), m/p-xylene (white with parallel dark grey stripes), C_6 ring closure (dark grey), alkenes (magenta), i-alkane (white with perpendicular dark grey stripes), and n-alkanes (white with parallel blue stripes) (a).C_6 ring closure selectivity (magenta) and dealkylation selectivity (blue) for all 6 excess*

K loaded catalysts, Pt/KMFI, and Pt/MFI (b). Reaction performance shown as productivity where poroductivity is defined as the moles of C_6 ring closure products /kg catalyst/h (c). Recylce runs of Pt/KMFI (KX-40) (magenta) and Pt/KL (blue), with performance displayed as productivity (d).

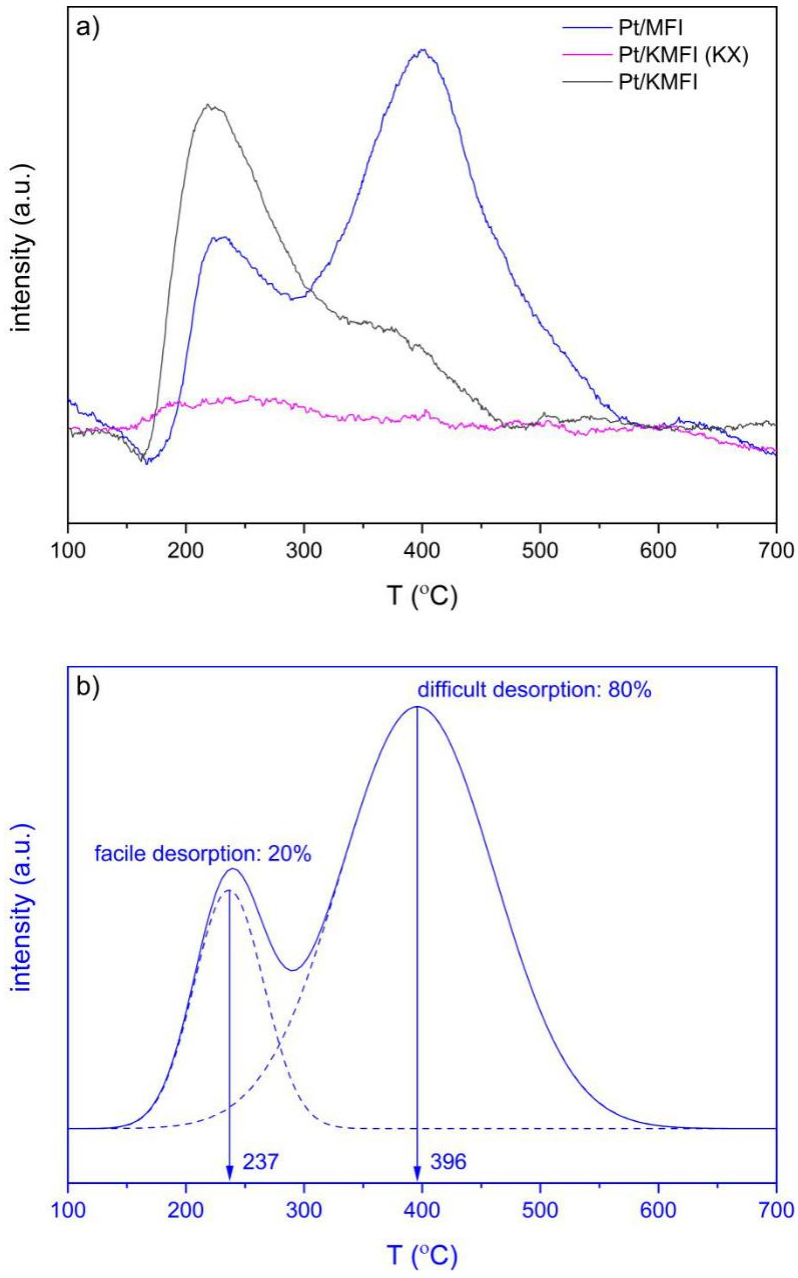

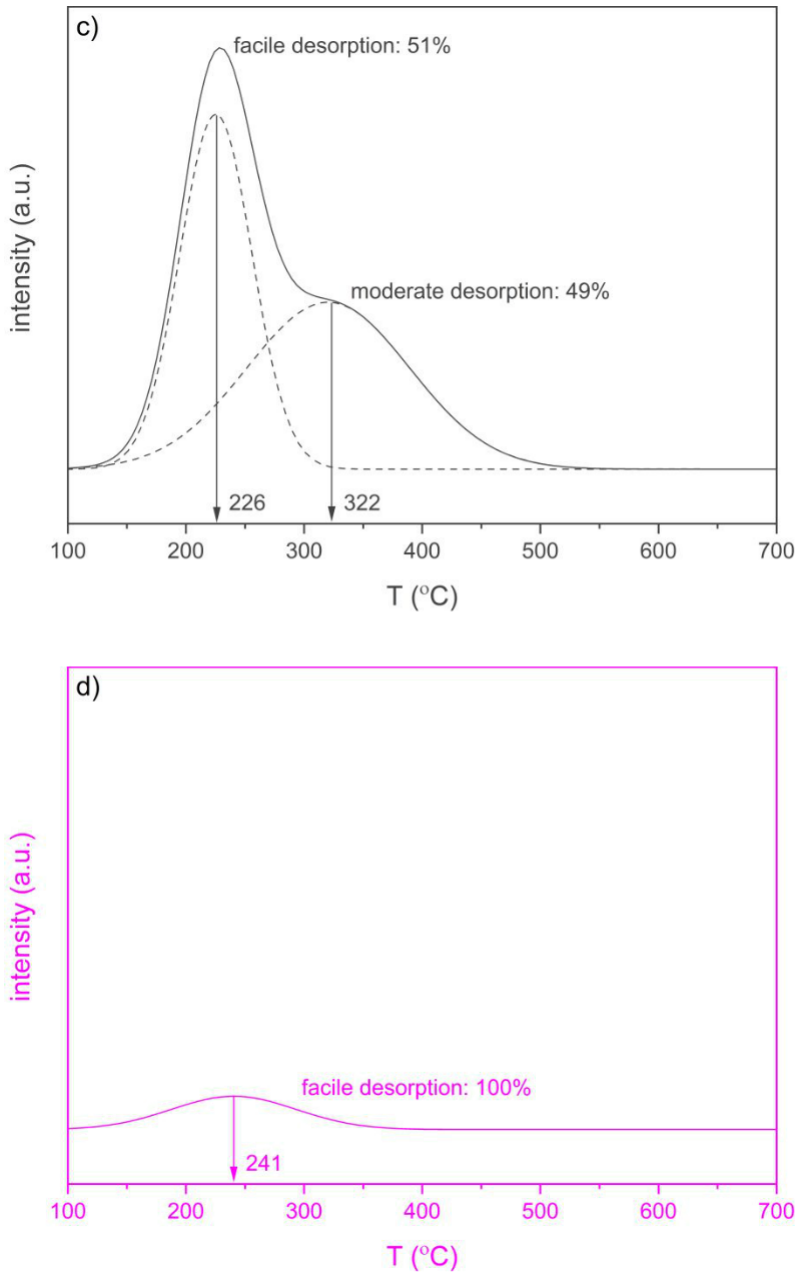

Fig. 4) NH_3-TPD profiles of catalysts. *Catalysts underwent temperature programmed desorption under NH_3 with detailed parameters shown in the methods. Pt/MFI is shown in blue (a) and (b). Pt/KMFI is represented in dark grey (a) and (c), and Pt/KMFI (KX-40) is represented in magenta (a) and (d).*

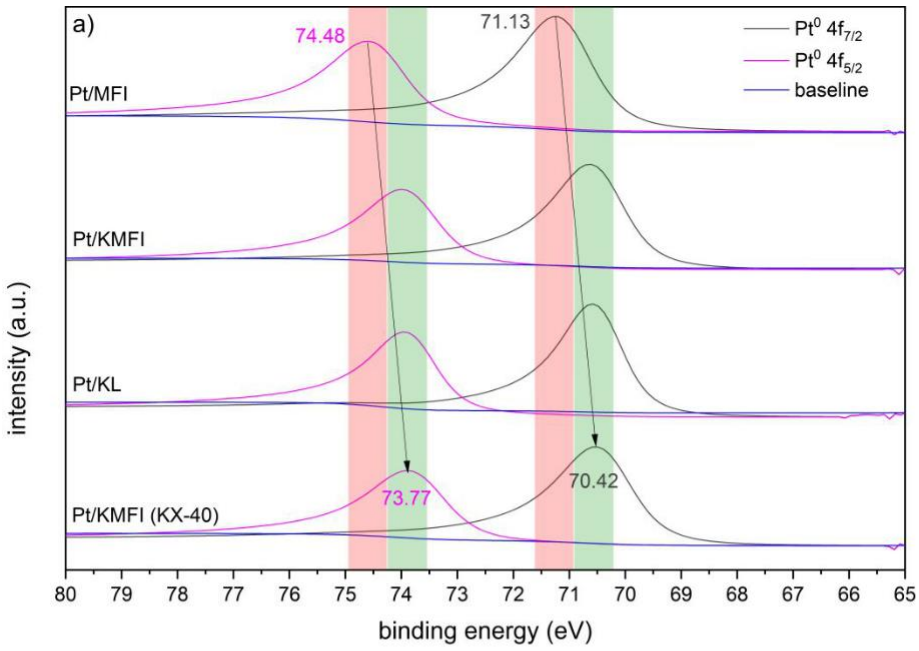
a)
74.48
71.13
Pt⁰ 4f7/2
Pt⁰ 4f5/2
baseline
Pt/MFI
Pt/KMFI
Pt/KL
Pt/KMFI (KX-40)
73.77
70.42
intensity (a.u.)
80 79 78 77 76 75 74 73 72 71 70 69 68 67 66 65
binding energy (eV)

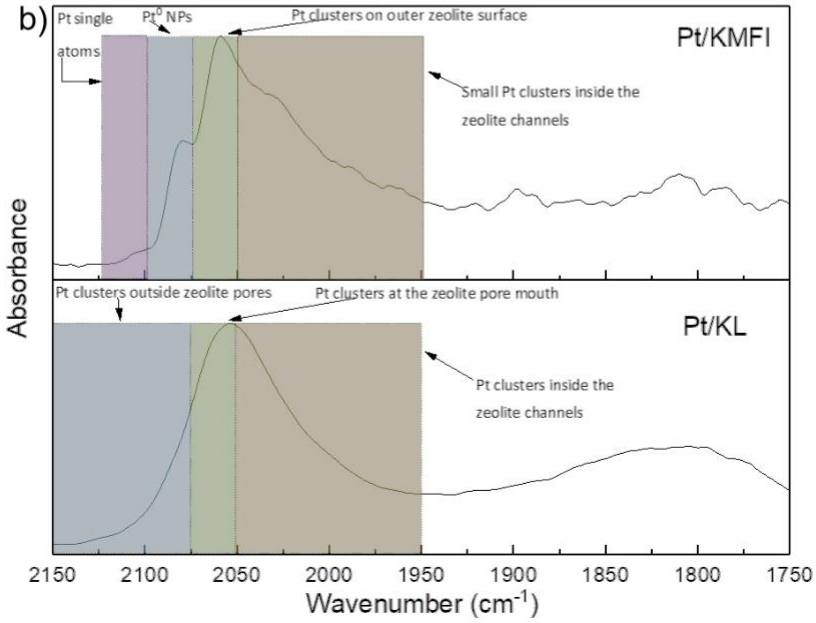
b)
Pt single atoms
Pt⁰ NPs
Pt clusters on outer zeolite surface
Pt/KMFI
Small Pt clusters inside the zeolite channels
Absorbance
Pt clusters outside zeolite pores
Pt clusters at the zeolite pore mouth
Pt/KL
Pt clusters inside the zeolite channels
2150 2100 2050 2000 1950 1900 1850 1800 1750
Wavenumber (cm-1)

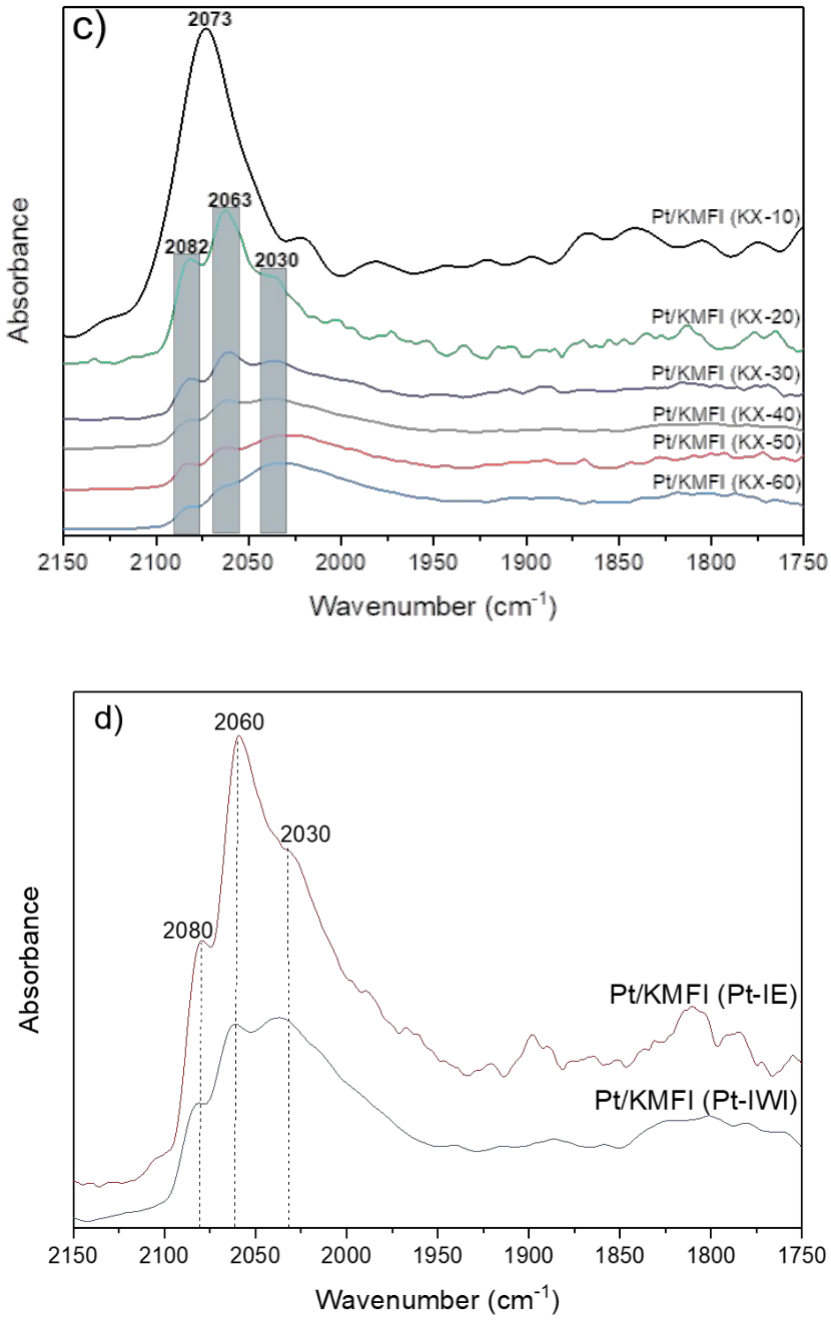

Fig. 5) XPS and CO-DRIFT spectra of Pt loaded supports with and without K presence. *Pt 4f regions of Pt/MFI, Pt/KMFI, Pt/KL, and Pt/KMFI (KX-40) catalysts (a). IR spectra of CO adsorbed on the Pt/KMFI and Pt/KL catalysts (b). IR spectra of CO adsorbed on (black) Pt/K-ZSM-5 (150:1), 10 mg/g K loaded during synthesis, IWI 1% Pt, (red) Pt/K-ZSM-5 (150:1), 20 mg/g K loaded during synthesis, IWI 1% Pt and (blue) Pt/K-ZSM-5 (150:1), 30 mg/g K loaded during*

synthesis, IWI 1% Pt catalysts. (c). IR spectra of CO adsorbed on the (blue) Pt/KMFI (Pt-IWI) and (black) Pt/KMFI (Pt-IWI) catalysts (d).

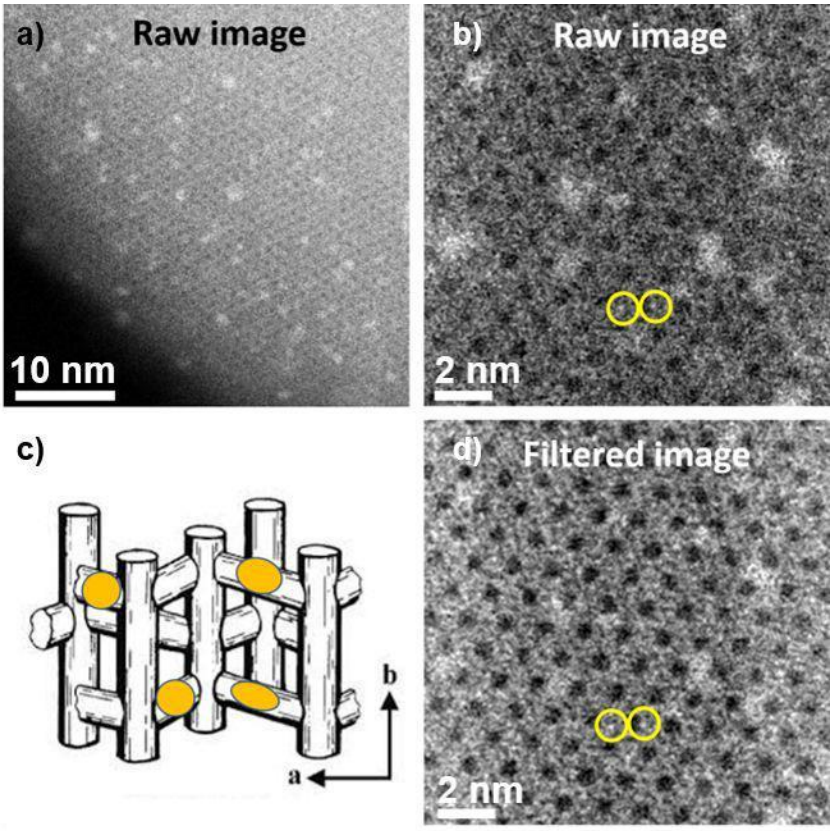

Fig. 6) STEM-HAADF images of Pt/KMFI and an illustrative cartoon of MFI channel structure. *Lower (a) and higher (b) magnification STEM-HAADF images of the Pt/KMFI (Pt-IWI) catalyst prepared using the incipient wetness impregnation method, viewed along the b-axis of the zeolite. While the channels along the b-axis can be clearly seen in (b) while the electron beam is focused onto the top surface, most of the Pt species appear to be out-of-focus, suggesting they are buried deeper into the zeolite and not blocking the main channels. Occasionally isolated Pt atomics can be observed, which are highlighted in yellow. (c) a cartoon demonstrates that the Pt clusters are likely to locate in the side channels in the MFI structure. (d) an Wiener filtered version of (b), showing the zeolite structure more clearly.*

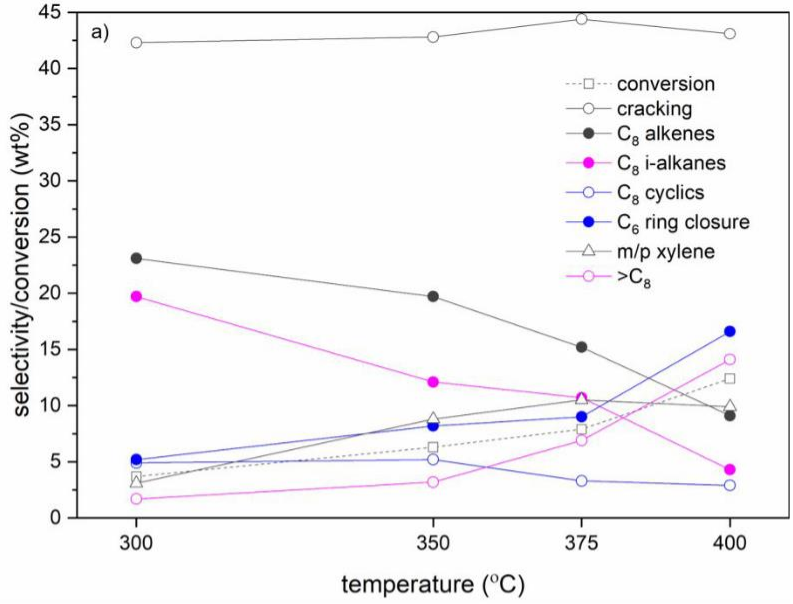
a)
selectivity/conversion (wt%)
temperature (°C)
conversion
cracking
C8 alkenes
C8 i-alkanes
C8 cyclics
C6 ring closure
m/p xylene
>C8

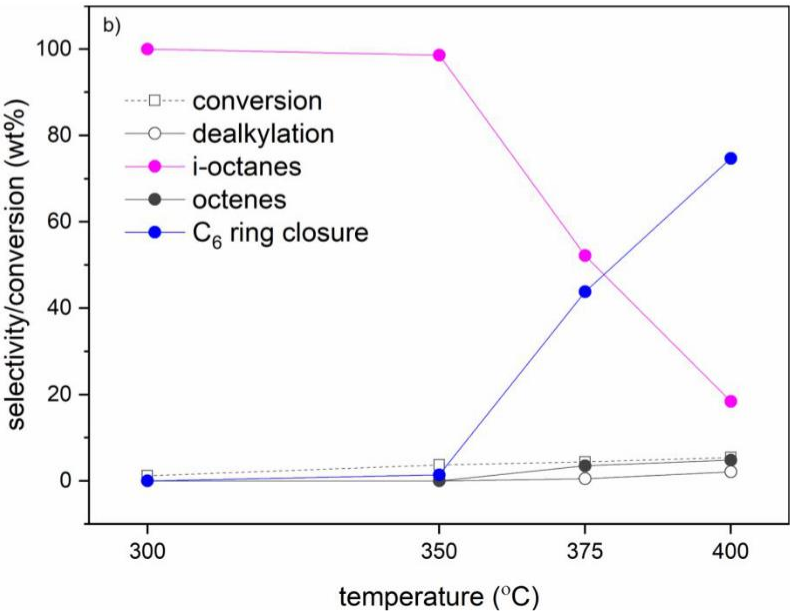
b)
selectivity/conversion (wt%)
temperature (°C)
conversion
dealkylation
i-octanes
octenes
C6 ring closure

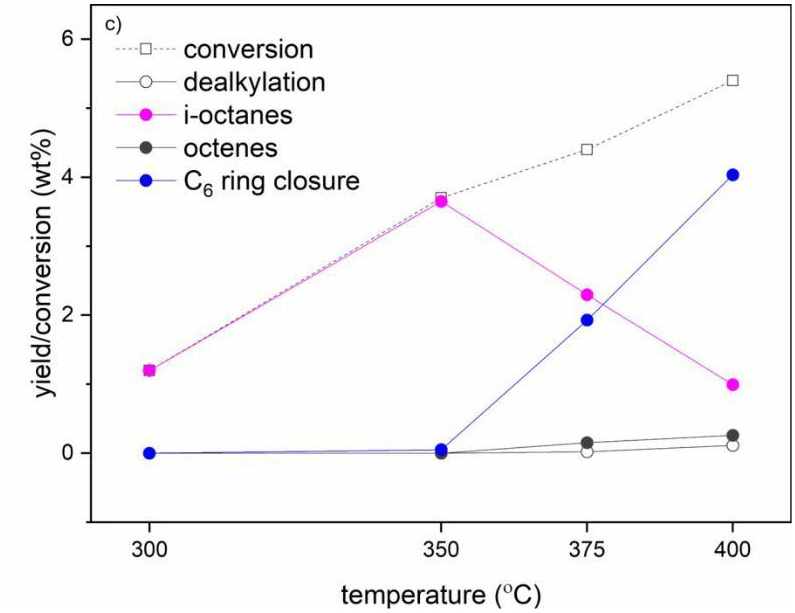

Fig. 7) Intermediate study of n-octane on Pt/MFI and Pt/KMFI (KX-40). *Products were analyzed on a selectivity basis (wt%) at 300, 350, 375, and 400°C and instantly quenched upon reaching the reaction temperature. Reaction over Pt/MFI (a). Reaction over Pt/KMFI (KX-40) (b). Performance of Pt/KMFI (KX-40) shown as yield (wt%) (c).*

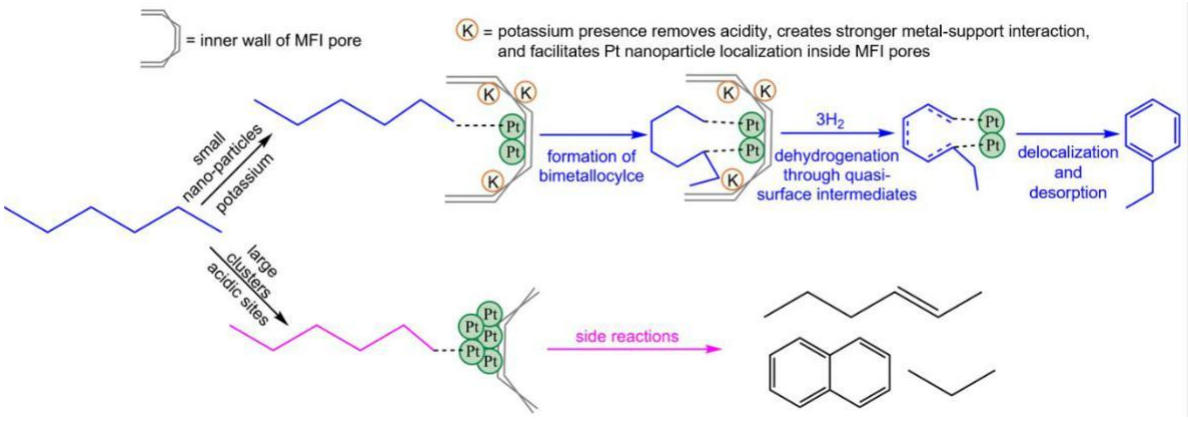

Fig. 8) Proposed mechanism for n-octane reaction over Pt nanoparticles inside the pores of KMFI and large cluster on the external surface of MFI. *Bimetallocycle mechanism for the reaction of n-octane over Pt/KMFI (KX) (blue). Pt cluster mechanism for the reaction of n-octane over Pt/MFI (magenta).*

For Table of Contents Only